Title

Identifying dominant environmental predictors of freshwater wetland methane fluxes across diurnal to seasonal time scales

Journal

Global Change Biology, 27(15)

ISSN

1354-1013

Authors

Knox, Sara H

Bansal, Sheel

McNicol, Gavin

et al.

Publication Date

2021-08-01

DOI

10.1111/gcb.15661

Peer reviewed

Identifying dominant environmental predictors of freshwater wetland methane fluxes across diurnal to seasonal time scales

Running title: Dominant predictors of wetland methane fluxes

Sara Helen Knox[1], Sheel Bansal[2], Gavin McNicol[3], Karina Schafer[4], Cove Sturtevant[5], Masahito Ueyama[6], Alex C. Valach[7], Dennis Baldocchi[7], Kyle Delwiche[3], Ankur R Desai[8], Eugenie Euskirchen[9], Jinxun Liu[10], Annalea Lohila[11,12], Avni Malhotra[3], Lulie Melling[13], William Riley[14], Benjamin R. K. Runkle[15], Jessica Turner[16], Rodrigo Vargas[17], Qing Zhu[14], Tuula Alto[12], Etienne Fluet-Chouinard[3], Mathias Goeckede[18], Joe R. Melton[19], Oliver Sonnentag[20], Timo Vesala[11], Eric Ward[21], Zhen Zhang[22], Sarah Feron[3,23], Zutao Ouyang[3], Pavel Alekseychik[24], Mika Aurela[12], Gil Bohrer[25], David I. Campbell[26], Jiquan Chen[27], Housen Chu[28], Higo J Dalmagro[29], Jordan P. Goodrich[26], Pia Gottschalk[30], Takashi Hirano[31], Hiroki Iwata[32], Gerald Jurasinski[33], Minseok Kang[34], Franziska Koebsch[33], Ivan Mammarella[11], Mats B. Nilsson[35], Keisuke Ono[36], Matthias Peichl[35], Olli Peltola[12], Youngryel Ryu[37], Torsten Sachs[30], Ayaka Sakabe[38], Jed Sparks[39], Eeva-Stiina Tuittila[40], George L Vourlitis[41], Guan Xhuan Wong[13], Lisamarie Windham-Myers[42], Ben Poulter[43], Robert B. Jackson[3,44,45]

[1] Department of Geography, The University of British Columbia, Vancouver, British Columbia, Canada
[2] U.S. Geological Survey, Northern Prairie Wildlife Research Center, 8711 37th St Southeast, Jamestown, ND 58401 USA
[3] Department of Earth System Science, Stanford University, Stanford, California
[4] Department of Earth and Environmental Science, Rutgers University Newark, NJ
[5] National Ecological Observatory Network, Battelle, Boulder, CO, USA
[6] Graduate School of Life and Environmental Sciences, Osaka Prefecture University
[7] Department of Environmental Science, Policy and Management, University of California, Berkeley, CA, USA
[8] Dept of Atmospheric and Oceanic Sciences, University of Wisconsin-Madison, Madison, WI 53706 USA
[9] University of Alaska Fairbanks, Institute of Arctic Biology, Fairbanks, AK, USA
[10] U.S. Geological Survey, Western Geographic Science Center, Moffett Field, CA, USA
[11] Institute for Atmospheric and Earth System Research/Physics, Faculty of Science, University of Helsinki, Helsinki, Finland
[12] Climate System Research, Finnish Meteorological Institute, PO Box 503, 00101 Helsinki, Finland
[13] Sarawak Tropical Peat Research Institute, Sarawak, Malaysia
[14] Earth and Environmental Sciences Area, Lawrence Berkeley National Lab, Berkeley, California

[15] Department of Biological & Agricultural Engineering, University of Arkansas, Fayetteville, Arkansas 72701, United States
[16] Freshwater and Marine Science, University of Wisconsin-Madison
[17] Department of Plant and Soil Sciences, University of Delaware, Newark, DE, USA
[18] Department of Biogeochemical Signals, Max Planck Institute for Biogeochemistry, Jena, Germany
[19] Climate Research Division, Environment and Climate Change Canada, Victoria, B.C., Canada
[20] Université de Montréal, Département de géographie, Université de Montréal, Montréal, QC H2V 0B3, Canada
[21] U.S. Geological Survey, Wetland and Aquatic Research Center, Lafayette LA
[22] Department of Geographical Sciences, University of Maryland, College Park, MD 20740, USA
[23] Department of Physics, University of Santiago, Santiago de Chile, Chile
[24] Natural Resources Institute Finland (LUKE), Latokartanonkaari 9, 00790 Helsinki, Finland
[25] Department of Civil, Environmental & Geodetic Engineering, Ohio State University
[26] School of Science, University of Waikato, Hamilton, New Zealand
[27] Department of Geography, Environment, and Spatial Sciences, & Center for Global Change and Earth Observations, Michigan State University, East Lansing, MI
[28] Climate and Ecosystem Sciences Division, Lawrence Berkeley National Lab
[29] Universidade de Cuiaba, Cuiaba, Mato Grosso, Brazil
[30] GFZ German Research Centre for Geosciences, Telegrafenberg, 14473 Potsdam, Germany
[31] Research Faculty of Agriculture, Hokkaido University
[32] Department of Environmental Science, Faculty of Science, Shinshu University
[33] University of Rostock, Rostock, Germany
[34] National Center for Agro Meteorology, Seoul 08826, South Korea
[35] Dept. of Forest Ecology and Management, Swedish University of Agricultural Sciences, 901 83 Umeå, Sweden
[36] Institute for Agro-Environmental Sciences, National Agriculture and Food Research Organization, Tsukuba, Japan
[37] Department of Landscape Architecture and Rural Systems Engineering, Seoul National University, Seoul 08826, South Korea
[38] Kyoto University, Kyoto, 606-8502, Japan
[39] Department of Ecology and Evolutionary Biology, Cornell, Ithaca, NY
[40] School of Forest Sciences, University of Eastern Finland, Joesnuu, Finland
[41] California State University San Marcos, San Marcos, CA, USA
[42] U.S. Geological Survey, Water Mission Area, 345 Middlefield Road, Menlo Park, CA, 94025
[43] Biospheric Sciences Laboratory, NASA Goddard Space Flight Center, Greenbelt, Maryland
[44] Woods Institute for the Environment, Stanford University, Stanford, California
[45] Precourt Institute for Energy, Stanford University, Stanford, California

*Corresponding author: Sara H. Knox, Tel: +1 (604) 833-0999; email: sara.knox@ubc.ca
Article type: Primary Research Articles

Keywords: Wetlands, methane, eddy covariance, synthesis, predictors, generalized additive modeling, mutual information, random forest, time scales, lags

Abstract:

While wetlands are the largest natural source of methane (CH_4) to the atmosphere, they represent a large source of uncertainty in the global CH_4 budget due to the complex biogeochemical controls on CH_4 dynamics. Here we present, to our knowledge, the first multi-site synthesis of how predictors of freshwater wetland CH_4 fluxes (FCH4) vary across wetland types at diel, multiday (synoptic), and seasonal time scales. We used several statistical approaches (correlation analysis, generalized additive modeling, mutual information, random forests) in a wavelet-based multiresolution framework to assess the importance of environmental predictors, nonlinearities and lags on FCH4 across 23 eddy covariance sites. Seasonally, soil and air temperature were dominant predictors of FCH4 at sites with smaller seasonal variation in water table depth (WTD). In contrast, WTD was the dominant predictor for wetlands with smaller variations in temperature (e.g., seasonal tropical/subtropical wetlands). Changes in seasonal FCH4 lagged fluctuations in WTD by ~17 ± 11 days, and lagged air and soil temperature by median values of 8 ± 16 and 5 ± 15 days, respectively. Temperature and WTD were also dominant predictors at the multiday scale. Atmospheric pressure (PA) was another important multiday scale predictor for peat dominated sites, with drops in PA coinciding with synchronous releases of CH_4. At the diel scale, synchronous relationships with latent heat flux and vapor pressure deficit suggest that physical processes controlling evaporation and boundary layer mixing exert similar controls on CH_4 volatilization, and suggest the influence of pressurized ventilation in aerenchymatous vegetation. In addition, 1-4 hour lagged relationships with ecosystem photosynthesis indicate recent carbon substrates, such as root exudates, may also control FCH4. By addressing issues of scale, asynchrony, and nonlinearity, this work improves understanding of the predictors and

116 timing of wetland FCH4 that can inform future studies and models, and help constrain wetland
117 CH_4 emissions.

1. Introduction

Methane (CH_4) is responsible for almost one quarter of the cumulative radiative forcing since the start of the industrial revolution (Etminan et al., 2016). As the largest natural source to the atmosphere, wetlands are responsible for ~30% of global CH_4 emissions, but their contribution to the global CH_4 budget is highly uncertain (Bridgham et al., 2013; Jackson et al., 2020; Saunois et al., 2020). The complexity of wetland CH_4 exchange, which is the net result of CH_4 production, consumption, and transport, makes interpreting and predicting fluxes challenging (Bridgham et al., 2013).

Previous site-level (Chu et al., 2014; Desai et al., 2015; Pugh et al., 2018; Chang et al., 2019) and synthesis studies (Moore & Dalva, 1993; Updegraff et al., 2001; Olefeldt et al., 2013; Turetsky et al., 2014; Treat et al., 2018; Knox et al., 2019; Peltola et al., 2019) of wetland CH_4 exchange have improved understanding of the abiotic and biotic controls on wetland CH_4 fluxes (FCH4). These studies established that temperature, water table position, air pressure and atmospheric turbulence, sediment biogeochemistry, and vegetation often dominate as coarse controls on net FCH4 from wetlands, with distinct controls varying by wetland type (Lai, 2009; Bridgham et al., 2013; Olefeldt et al., 2013; Turetsky et al., 2014; Treat et al., 2018; Wen et al., 2018). Both air and soil temperature (TA and TS, respectively) can influence FCH4, with the former dominating physical processes of diffusive transport in plants and the latter strongly influencing microbial processes controlling CH_4 production and oxidation and subsequent soil diffusion and ebullition; thus, both often emerge as dominant predictors of FCH4 within and across sites (Knox et al., 2019; Morin, 2019). Water table depth (WTD) governs the reduction-oxidation (redox) zones that determine CH_4 production and oxidation (Moore & Knowles, 1989; Bubier et al., 1995; Malhotra & Roulet, 2015; Perryman et al., 2020, etc.). Physical processes

142 such as turbulent conditions and atmospheric pressure (PA) fluctuations can influence the
143 transport of CH_4 from the soil profile into the atmosphere, particularly in porous peat soils where
144 ebullition is often the primary CH_4 transport mechanism during the pressure-falling phase (Sachs
145 et al., 2008; Nadeau et al., 2013; Ueyama et al., 2020b). Biological factors such as plant
146 community type and primary production also influence CH_4 production and consumption
147 through a variety of mechanisms including: supplying labile carbon compounds that fuel
148 methanogenesis (Christensen et al., 2003; Tittel et al., 2019); enhancing oxygen transport into
149 anoxic soil layers via aerenchyma thereby supporting rhizosphere CH_4 oxidation (Laanbroek,
150 2010); and mediating transport of CH_4 to the atmosphere via aerenchyma, allowing CH_4 to
151 bypass potential oxidation in surface soils (Knoblauch et al., 2015; Kwon et al., 2017; Villa et
152 al., 2020).

153 Determining the environmental controls on FCH4 is critical for understanding and
154 modeling these fluxes. In addition to considering direct, mechanistic drivers of methanogenesis,
155 methanotrophy and CH_4 transport (e.g., temperature, WTD, PA) (c.f., Table 1), there are also
156 benefits to understanding alternative variables that are strongly correlated with FCH4 even if
157 such variables (e.g., latent heat (LE)) are indirectly linked to FCH4 (Table 1). These indirect
158 variables can be measured alongside FCH4 and its direct drivers to help capture the complex and
159 nonlinear relationships between environmental drivers and FCH4 and can describe similar
160 processes to those influencing CH_4 exchange (Morin et al., 2014), and therefore are well-suited
161 for inclusion in data-driven FCH4 models.

162 While a general concept of the overall controls on wetland FCH4 has been established,
163 understanding the functional controls on FCH_4 is highly influenced by the temporal and spatial
164 scales of measurements (Turetsky et al., 2014). In particular, until recently, data and synthesis

165 studies were largely biased toward chamber-based measurements from temperate and northern
166 high-latitude regions (Olefeldt et al., 2013; Turetsky et al., 2014). However, manual chamber
167 measurements are typically discrete in time and space, and therefore may not capture the full
168 spatiotemporal range of CH_4 dynamics, limiting the investigation of the underlying drivers and
169 patterns of FCH4 in wetlands (Morin, 2019).

170 Eddy covariance (EC) flux towers provide ecosystem-scale, noninvasive and near-
171 continuous measurements of the exchange of mass (e.g., carbon dioxide (CO_2), CH_4, water) and
172 energy between the land surface and the atmosphere (Baldocchi, 2014). Methane exchange in
173 wetlands often involves nonlinear and asynchronous processes across multiple time scales
174 (Sturtevant et al., 2016; Schaller et al., 2019). The continuous, high-frequency nature of EC
175 measurements along with supporting biophysical measurements offer promising datasets for
176 improving understanding of wetland FCH4 over multiple timescales. For example, water-level
177 fluctuations correspond with pulses of CH_4 with hourly to daily delays (Hatala et al., 2012a), but
178 also inhibit FCH4 across a range of time scales (Sturtevant et al., 2016; Koebsch et al., 2015).
179 However, despite the fact that many of these processes and time scales are poorly characterized
180 at the ecosystem scale, they are important for predicting FCH4 and, therefore, are critical to
181 include in data-driven and process-based models (Koebsch et al., 2015; Li et al., 2018). While
182 studies using EC flux data can elucidate these knowledge gaps, most studies focus on single
183 sites, thus limiting the scope of inference and generalization across multiple wetland types at
184 regional and global scales. Furthermore, given the complexity of wetland FCH4, more studies
185 explicitly questioning assumptions of linear, synchronous, and single-scale analyses are needed,
186 which can provide new insights into interpretations and predictions of CH_4 dynamics.

Robust statistical approaches are required to capture and describe CH_4 dynamics. Numerous statistical methods with known strengths and weaknesses have been used to describe and model FCH4, ranging from simple correlation analysis to more complex machine-learning algorithms (Genuer et al., 2010; Peltola et al., 2019; Kim et al., 2020). By implementing and comparing multiple statistical approaches, it is possible to evaluate how our understanding of the complex interactions between controls on FCH4 is influenced by the choice of statistical analysis (Trifunovic et al., 2020).

In this study, we take advantage of near-continuous EC measurements to elucidate the predictors and timing of wetland CH_4 flux dynamics. Here we use the term 'predictor' rather than 'driver' or 'control' since we are considering direct, indirect and coincident variables associated with FCH4 (c.f., Table 1). We leverage the FLUXNET-CH4 dataset (Knox et al., 2019; Delwiche et al., in review) and multiple statistical approaches to analyze measurements from 23 EC sites across the world (representing 107 site-years of data) to better constrain the dominant predictors of freshwater, non-tidal wetland FCH4 across time scales and wetland types. Specifically, we address the following questions: i) What are the dominant predictors of FCH4 at diurnal to seasonal time scales at each wetland? ii) How does the relative dominance of each predictor vary across wetland types? iii) Is the identification of dominant predictors of FCH4 influenced by the choice of statistical approach? iv) How important are nonlinearities and lags in interpreting FCH4?

2. Methods

2.1. Dataset and site description

Twenty-three sites from the FLUXNET-CH4 database (Table 2, Fig. 1) were selected for this analysis because they had at least one full year of FCH4 measurements and reported all

predictors of interest (Table 1). We only analyzed data for non-tidal, freshwater wetlands because FCH4 from tidal wetlands is influenced by additional factors such as salinity, sulfate reduction, and tidal action (Seyfferth et al., 2020). Data standardization, gap-filling, and partitioning of net ecosystem exchange (NEE) of CO_2 for the FLUXNET-CH4 dataset are described in detail in Knox et al. (2019) and Delwiche et al. (in review). Here we considered physical predictors of FCH4 such as TA, TS, WTD, PA, incoming shortwave radiation (SW_IN), vapor pressure deficit (VPD), and wind direction (WD), biological predictors such as gross primary productivity (GPP), NEE, or ecosystem respiration (RECO), and coincident, indirect variables such as LE, to understand which variables are strongly correlated with FCH4 and under what conditions and time scales (Table 1). When more than one observation depth for TS was available, we selected TS at the depth where the statistical dependence of FCH4 on TS was highest (see Section 2.2.3). As noted above, here we use the term 'predictor' rather than the terms 'driver' or 'control' since several of the variables considered here do not have a direct influence on CH_4 production, consumption and/or transport, but rather reflect variables that represent a proxy or are correlated with processes that have a direct influence on FCH4. However, in the Discussion we emphasize which predictors represent direct drivers of FCH4 and which reflect proxies (c.f., Table 1).

Sites were classified into bog, fen, marsh, swamp, rice paddy, and drained wetland based on site-specific literature (Delwiche et al., in review) (Table 2, Fig. 1). Climate was extracted and modified from Olson et al. (2001) using site coordinates and includes boreal, temperate, and tropical/subtropical. No tundra sites were included in this analysis due to the lack of key ancillary variables (e.g., WTD) in the FLUXNET-CH4 database. Management regimes included natural, managed, and restored freshwater wetlands (Table 2).

2.2. Within-site analysis of the dominant predictors of CH_4 fluxes

To investigate the complexity of wetland FCH4, we compared multiple statistical approaches to analyze the dominant predictors of FCH4 and evaluate whether findings of the most important predictors of FCH4 were consistent across approaches. We used methods commonly used in analyses of FCH4 and their drivers, ranging from simple linear correlation to more complex methods such as generalized additive models (GAM), information theory, and random forests (RF). For each method, the goal was to identify and rank the importance of predictors of FCH4 (i.e., independent variables) to explain the variability of FCH4 (i.e., dependent variable).

Variable importance analyses using each of the four methods were first performed using daily mean data, a common time step for analyzing FCH4 (Turetsky et al., 2014; Rinne et al., 2018). Analyses were also performed on wavelet-decomposed data using half-hourly data, as described below, to assess how predictors vary across time scales (i.e., diel to seasonal time scales), as partitioning variability across scales can help isolate and identify important processes (Koebsch et al., 2015).

2.2.1. Wavelet-based time-scale decomposition

The maximal overlap discrete wavelet transform (MODWT) was used to decompose the time scales of variability in gap-filled FCH4 and explanatory variables (Sturtevant et al., 2016) (see Supporting Information for full details and implementation including treatment of gaps). The MODWT decomposes the time series into the detail added from progressively coarser to finer scales, and can be either summed or treated individually to explore patterns across scales. The detail in the half-hourly fluxes were reconstructed for dyadic scales 1 (2^1 measurements = 1 h) to 14 (2^{14} measurements = 341 days). We summed the detail over adjacent scales to yield four

general time scales of variation (Sturtevant et al., 2016). Time scales of variation included the "hourly scale" (1–2 h) representing short-term perturbations such as clouds passing overhead, the "diel scale" (4 h to 1.3 days) representing the diel cycles in radiation and temperature, the "multiday scale" (2.7 to 21.3 days) encompassing synoptic weather variability and shorter-term variations in water levels, and the "seasonal scale" (42.7 to 341 days) representing vegetation phenology, seasonal hydrological cycle, and the annual solar cycle. Data were wavelet decomposed into the hourly, diel, multiday, and seasonal scales with the Wavelet Methods for Time Series Analysis (WMTSA) using the Wavelet Toolkit in MATLAB (Cornish et al., 2003). We focused predominantly on the predictors of diel to seasonal time scales as the hourly wavelet scale is often dominated by noise (Hollinger & Richardson, 2005). As such, the hourly scale was only produced to show the distribution of FCH4 variability across time scales.

Since wavelet decomposition requires special treatment of gaps, we used gap-filled data from the FLUXNET-CH4 database for the wavelet decomposition. However, following wavelet decomposition, the original gaps were subsequently re-introduced prior to the analyses described below in all but the seasonal time scale to minimize biasing the results based on gap-filling algorithms (Sturtevant et al., 2016). Original gaps at the seasonal scale were not removed because gap lengths were small relative to this scale.

2.2.2. Linear correlation

A pairwise Pearson's linear correlation analysis between predictors and FCH4 was performed on all sites and time scales described above, with predictor importance represented by the coefficient of determination (Table S1). Log transformation was not performed as difficulties arise in interpreting log transformed variables. In addition, negative and zero values would need to be either discarded or manipulated for a log transformation and therefore skew the results. All

282 analyses were conducted in Matlab 2019a (Mathwork Inc., Natick, MA, USA). The linear
283 correlation was deemed significant at an α level of 0.05.

284 *2.2.3. Relative Mutual Information (IR)*
285
286 In information theory, mutual information (I), defines the average tendency for paired
287 states of two variables (e.g., X and Y) to coexist (Fraser & Swinney, 1986). Computed from the
288 marginal and joint probability distributions of X and Y, relative mutual information (IR_{XY})
289 characterizes the proportion of bits required to represent Y that is redundant given the knowledge
290 of X. Put differently, it is a normalized measure of the statistical dependence of Y on X, with
291 larger values indicating higher dependence, or in this context, identifying a stronger link to
292 FCH4. A strength of I_{XY} lies in the lack of parametric assumptions about the relationships
293 between X and Y, and therefore, it can address both linear and nonlinear interactions. The
294 strength of I_{XY} and IR_{XY} is further enhanced by adding a time lag (τ) to these metrics, thereby
295 allowing us to identify both synchronous and asynchronous interactions. A "synchronous"
296 interaction is defined as one in which the maximum IR_{XY} is found at $\tau = 0$ (i.e., zero-time lag),
297 indicating that variations in Y are most related to simultaneous variations in X. Otherwise, the
298 interaction is characterized as "asynchronous", where maximum IR_{XY} at $\tau > 0$ indicates that the
299 fluctuations in Y lagged variations in X, while maximum IR_{XY} at $\tau < 0$ implies that variations in
300 Y lead variations in X. As such, mutual information can identify both the statistical strength (i.e.,
301 predictor importance) and asynchrony of complex biosphere-atmosphere interactions, such as
302 wetland FCH4 (Sturtevant et al., 2016).

303 IR between FCH4 (X) and biophysical predictors (Y) of interest was calculated for both
304 daily mean data and wavelet decomposed data over a range of time lags (τ) using version 1.5 of
305 the ProcessNetwork Software (Table S2) (Ruddell et al., 2008). Details on the lags,

306 discretization, statistical significance and bias correction are provided in the Supporting
307 Information.

308 *2.2.4. Generalized additive models (GAMs)*
309
310 The third method used to assess important predictors of FCH4 were GAMs. FCH4 often
311 follows nonlinear relationships with various potential predictor variables. Unlike linear
312 correlation analysis, GAMs have the capability of describing these nonlinear relationships and
313 treating the degree of nonlinearity as a quantity to be estimated. We developed GAMs of FCH4
314 using each predictor individually. Relative predictor importance was determined by comparing
315 the deviance explained among predictors (Table S3). All GAMs were implemented using the
316 *mgcv* package in R version 3.6.2 (Wood, 2011), with details provided in the Supporting
317 Information.

318 *2.2.5. Random forests (RF)*

319 The last method used to assess variable importance and the dominant predictors of FCH4
320 was random forests (RF), which is a machine learning algorithm that grows an ensemble of
321 decision trees (Breiman, 2001). A strength of decision trees is that this approach can reproduce
322 nonlinearities among multiple predictor variables to explain FCH4. For each tree, data are
323 successively split at decision nodes to minimize variance in the resulting branches. Predictor
324 variables can be considered at multiple decision nodes within a single tree, allowing the RF
325 algorithm to thoroughly explore possible predictor conditions. Moreover, the RF algorithm is
326 less prone to issues of overfitting associated with single trees because it grows an ensemble
327 (forest) of decision trees and each tree is trained using randomly drawn (bagged) subsamples of
328 the data.

A RF algorithm was trained for each site using the *ranger* package in R (Wright & Ziegler, 2017; R Core Team, 2019) with details provided in the Supporting Information. We ranked predictors using permutation importance, which avoids bias of other methods (Strobl et al., 2007) and scaled importances for site comparisons (Table S4). We also provide out-of-bag model fit metrics (coefficient of determination, mean absolute error, and bias) as a further evaluation of relative confidence in results between sites (Fig. S13, Fig. S14).

2.2.6. Variable importance standardization

Each statistical method was used to provide a numeric ranking of variable importance, which we used to estimate dominant FCH4 predictors (i.e., the highest ranked covariates) and assess how predictors vary between statistical methods. However, the statistical approaches have different scales for variable importance scores and different ranges between sites. As such, variable importance metrics for each method were normalized between zero and one, and therefore for all sites and methods, the strongest predictor has a value of one and the lowest a value of zero. This normalization ensures comparability in scores across wetland sites and methods.

2.3. Visualizing and cross-site synthesis of the dominant predictors of CH_4 fluxes

To distill the information generated from the variable importance metrics described above, heatmaps and principal component analysis (PCA) were used to visualize and assess predictor patterns across sites and wetland types. Here we used the heatmap.2 function in *gplots* R package (Warnes et al., 2019) to generate a heatmap (without cluster analysis) of the normalized variable importance metrics described above to help visualize dominant predictors across sites.

PCA analysis was used to summarize and visualize the information contained in the variable importance analysis. For each method, we compressed the standardized variable importance scores generated using the statistical approaches described in Sections 2.2.2-2.2.5 into two principal components. The distributions of sites on the principal components visualize how strongly FCH4 at each site was regulated by the environmental predictors. PCA analysis was done using the *prcomp* function in base R. Columns of the normalized matrices were centered so that the mean of each column was equal to zero (Abdi & Williams, 2010).

3. Results

3.1. Magnitude of FCH4 and time scales of variability

FCH4 exhibited a wide range of magnitude across the 23 sites, with median FCH4 varying from 0.5 to 541 nmol m^{-2} s^{-1} (Table 2). Median FCH4 averaged within wetland types was highest in marshes, followed by rice, fens, bogs, and swamps.

FCH4 exhibited strong variation across time scales (Fig. 2). The seasonal time scale tended to dominate FCH4 variability across wetland sites, although it was notably lower in some tropical/subtropical sites where the seasonal variability of multiple biophysical predictors (e.g., radiation, temperature, GPP) tended to be much lower than in temperate and boreal sites. The variation in FCH4 at multiday and hourly scales was generally low. However, some sites with low fluxes tended to have higher variation at the hourly scale (e.g., FI-Si2 and US-Uaf) due to the higher signal to noise ratio (Hollinger & Richardson, 2005).

Variation at the diel scale also varied across sites. Sites with high diel FCH4 variation typically showed a diurnal pattern of highest fluxes during late-morning to mid-afternoon and lower fluxes at night (Fig. 2, Fig. S1). Nonetheless, some sites with considerable variation at the diel scale exhibited different diurnal patterns (Fig. S1). At some sites, the proportion of variance

in FCH4 at the diel scale appeared large despite a lack of a typical diurnal pattern (e.g., ID-Pag, FI-Si2, MY-MLM, US-Uaf). This was largely attributed to the fact that at these sites variation at other scales (e.g., seasonal) was low (Fig. 2) and/or the magnitude of FCH4 was low (Table 2).

3.2. Dominant predictors of FCH4 across time scales

3.2.1. Summary across sites, time scales and methods

To assess the dominant predictors at each time scale, we averaged normalized variable importance scores across sites for each method (Table 3). At the seasonal scale, TS always ranked as the dominant predictor. TA alternated as either the second or third most important predictor along with LE or NEE. Overall, the different approaches tended to converge on the top predictors, with each of these dominant predictors explaining on average >50% of the variance in seasonal FCH4 based on the linear correlation and GAM analyses (Tables S1 and S3).

Similar to the seasonal scale, there was also general consistency between methods at the multiday scale, with all approaches again identifying temperature (TS and/or TA) in the top three predictors (Table 3). Other key predictors that emerged at the multiday scale included PA, LE, WTD, and wind direction (WD). While overall less of the variability in multiday FCH4 was explained by each of the individual predictors, the top predictor at each site generally explained between 10 and 50% of the variance in multiday FCH4 (Table S1 and S3), with site-level R^2 > 0.95 for the RF model with all predictors (Fig. S13).

At the diel scale, all approaches identified LE and NEE as the top two predictors of FCH4, and with GPP or SW_IN as the third most important predictor depending on the method (Table 3). While the explanatory power of individual predictors was lowest at the diel scale, predictors did explain up to 50% of the variability in FCH4 for sites with a typical diurnal pattern (i.e., lower fluxes at night and higher during the day) (Table S1 and S3).

Daily averaged data are often used for analysis of FCH4 variation at the seasonal scale (Chu et al., 2014; Rinne et al., 2018). However, unlike wavelet seasonal transformed data, daily averages also include influences from other time scales of variation. As such, although temperature (TS or TA) was consistently found to be the top driver across methods at this time step, other variables such as GPP, NEE and WTD, which were identified as key controls of FCH4 at the multiday and diel scales, were also identified in the top three drivers for daily averaged data (Table 3).

Given the consistent patterns across methods (Table 3), we focus on the findings of the IR method for the remainder of the results. The IR approach is explicitly designed to identify both synchronous and asynchronous relationships (Sturtevant et al., 2016), representing an advantage over the other statistical methods where accounting for lags is possible but it is not among their inherent strengths. However, results from the other statistical approaches are presented as necessary (primarily in the SI) to show consistency or highlight differences in the methods.

3.2.2. Patterns within and across sites at the seasonal scale

Figure 3 shows a detailed picture of the dominant predictors within and across sites determined by maximum IR between FCH4 and biophysical variables. The heatmap at the seasonal scale for both maximum IR (Fig. 3a) and synchronous IR (Fig. S2a) shows that temperature (TS or TA) was the dominant predictor across the majority of sites at this scale, with LE, NEE, and GPP also among top predictors, corroborating the broader patterns across sites shown in Table 3. The dominance of temperature, LE, NEE, and GPP was also apparent in the other statistical approaches (Fig. S3). However, Fig. 3a and Fig. S2a also revealed other patterns which were obscured when averaging variable rankings across sites; notably, WTD was a

dominant predictor at the swamp and drained sites and two of the rice paddy sites. The importance of WTD at these sites was also consistent across statistical methods (Fig. S3).

The importance of temperature and WTD was also evident in the PCA analysis of IR results (Fig. 4). Sites clustered along PC1 (29% of explained variance) which corresponds predominantly with WTD, TA, LE and VPD (highly correlated with TA) as dominant predictors of FCH4 at the seasonal scale (Table S5). This clustering by wetland type further supports the finding above that, while temperature was a dominant predictor at most sites, WTD was a key control at the swamp, drained but seasonally inundated, and two of the rice paddy sites. Sites where WTD is a dominant predictor at the seasonal scale also tended to have a greater ratio in the variation of WTD relative to TA (Fig. 4). This visible clustering along axes of WTD and temperature (and variables correlated with temperature) was also apparent in the PCA analysis of the results from the linear correlation, GAM, and RF analyses (Fig. S4), again supporting the findings of the IR analysis of the dominant predictors of FCH4 at the seasonal scale (Table 3, Fig.S3, Fig. S4).

The results of the PCA analysis also suggested other clusters across wetland types. Fens and most bogs tended to cluster together along PC2 in the bottom right corner of the scatter plot indicating the importance of GPP and RECO as secondary predictors of FCH4 in these wetland types (Fig. 4, Fig. 3a, Table S5). However, except for GAM, similar clustering for bogs and fens was less apparent in the other statistical approaches (Fig. S4).

For sites where WTD was among the higher ranked predictors (the swamp and drained sites, two rice paddy sites, and the bog NZ-Kop; Fig. S6), seasonal FCH4 lagged WTD by an average of approximately 17 ± 11 days (standard deviation) (Fig. 5a, Fig. S5, Fig. S6). The lag at peak $IR_{WTD,FCH4}$ at individual sites ranged from 2 to 35 days (Fig.5a, Fig. S5, Fig. S6). The

median lag between seasonal FCH4 and TA was 8 ± 16 days (Fig. 5b), and the median lag with TS was 5 ± 15 days (Fig. 5c). These findings suggest a more synchronous relationship between FCH4 and temperature at the seasonal scale relative to WTD (Fig. 5). As noted in the methods, here we selected TS at the depth where $IR_{TS,FCH4}$ was greatest. We hypothesize this is the depth where CH_4 production was greatest but acknowledge the lack of information on the depth profile of CH_4 oxidation and labile carbon supply. With respect to negative lags with TS, a negative lag does not indicate that seasonal FCH4 began to increase before TS; for all sites and site years, seasonal FCH4 began to increase after TS, and therefore negative lags with TS reflected the fact that seasonal FCH4 peaked prior to TS and/or began to decrease prior to the decrease in TS at the end of the growing season (Fig. S7). Lags were also observed with respect to other top predictors of seasonal FCH4 (Fig. 5d,e), where both LE and GPP tended to increase and/or peak prior to FCH4 (Fig. S8). The median lag between FCH4 and LE was 17 ± 18 days (Fig. 5d), while FCH4 lagged GPP by 12.5 ± 23 days (Fig. 5e).

3.2.3. Patterns within and across sites at the multiday scale

WTD, TA, and PA were among the top predictors at the multiday scale (Table 3, Table S6, Fig. 3b, Fig. 4b) and were generally consistent across statistical approaches. However, the relationships with WTD and PA were less apparent for linear correlation analysis and GAMs, respectively (Table S6, Fig. S9). While clustering across wetland types was less pronounced at the multiday scale (Fig, 4b, Fig. S10), some patterns emerged. Notably, PA was in the top three predictors at several peat-dominated sites, including bogs, fens, a peat swamp, and a restored marsh underlain by peat (Fig. 3a, Fig. S10). The relationship between FCH4 and PA was near-synchronous. Although Fig. 6a suggests that FCH4 slightly led drops in PA (on the order of ~4 ± 2 hours), these lags are not significantly different from zero at the multiday scale (Sturtevant et

al., 2016). As such, drops in PA coincided with synchronous releases of FCH4 (Fig. 6b, Fig. S10). Pressure fluctuations on the order of 0.5 to 2 kPa resulted in pulses of CH_4 on the order of 5 to 100 nmol m^{-2} s^{-1}, with larger pulses in CH_4 at high emitting sites (Fig. S10).

Similar to the relationship with PA, there was a near-synchronous relationship between multiday temperature (both TA and TS) and FCH4 (Fig. 6c). WTD was also one of the top predictors at several sites (Fig. 3b, Fig. 4b, Fig S9) but had a slightly more complex, nonlinear relationship than those described previously at the multiday scale. Examination of $IR_{WTD,FCH4}$ with lag (Fig. 6e) generally showed both a primary interaction where variation in FCH4 slightly led variation in WTD (a lag of ~8 hours), and a secondary interaction where FCH4 lagged WTD. As illustrated for US-Tw1, the wavelet detail reconstruction for these variables (Fig. 6f) showed pulses in CH_4 generally coinciding or occurring slightly before minima in WTD. There also tended to be a secondary peak in $IR_{WTD,FCH4}$ on the order of 4-6 days (Fig. 6e). This secondary lagged interaction was frequently the result of lower FCH4 after a subsequent rise in WTD (Fig. 6f). The one exception to this pattern was at the rice paddy site (US-Twt), where IR as a function of lag only had a single peak (Fig. 6e), with maximum $IR_{WTD,FCH4}$ occurring at a lag of ~5 days.

3.2.4. Patterns within and across sites at the diel scale

Some sites had more variation at the diel scale than others. Sites which exhibited a typical diurnal pattern primarily included fens, marshes, swamps, and rice paddies, with amplitudes in the diel pattern ranging between ~8 to 172 nmol m^{-2} s^{-1} (Fig. 7, Fig. S1). While not all fens, marshes, and swamps exhibited diel variation, only one of the bogs had a typical diurnal pattern (Fig. 7, Table 2). All sites with a typical diurnal pattern had aerenchymatous vegetation and only JP-BBY had mosses (*Sphagnum*) present.

Across statistical methods, top predictors of FCH4 at the diel scale included LE, NEE, GPP, although in some cases SW_IN and VPD were also among the top predictors of diel FCH4 (Table 3). Of the sites characterized by a typical diurnal pattern the dominant relationship observed were between FCH4 and LE (5 sites), GPP (3 sites), net ecosystem production (NEP, or negative NEE) (2 sites), VPD (1 site), and SW_IN (1 site) (Fig. 7). The relationship between FCH4 and LE was approximately synchronous (~ 0 hours), with lags ranging between -1 and 0.5 hours, and a median lag of 0 hours. Lags were slightly longer for the other biophysical predictors, ranging up to 4 hours for GPP, 3 hours for NEP, 2 hours for SW_IN and 1 hour for VPD.

While in most cases the mean diel pattern of the biophysical predictor with maximum IR closely matched that of FCH4, in some cases the diel patterns were less well aligned (e.g., DE-Zrk) (Fig. 7). This discrepancy occurs because IR reflects not only similarity in the shape of the diel pattern, but also in the magnitude of the diel variability (Fig. S11) (Sturtevant et al., 2016). For example, at DE-Zrk, the shape of the diel pattern in FCH4 appears to be more strongly related to VPD while the amplitude of the pattern was more closely related to GPP (Fig. S11). This discrepancy between the mean diel pattern of the biophysical predictor with maximum IR and FCH4 was observed in some other sites as well (e.g., KR-CRK; US-Twt); however, when considering synchronous relationships (i.e., = 0), in most cases the diel pattern in FCH4 closely matched that of LE or VPD (Fig. S12).

4. Discussion

Methane exchange in wetlands is complex, and often involves nonlinear and lagged interactions across a range of time scales (Sturtevant et al., 2016). While several studies have explored environmental controls on FCH4 across wetland types and biomes (Olefeldt et al.,

511 2013; Turetsky et al., 2014; Treat et al., 2018), this is the first multi-site synthesis study that
512 explores how predictors of non-tidal, freshwater wetland FCH4 vary across time scales, assesses
513 how the relative dominance of these predictors vary across wetland types, and identifies
514 nonlinear and asynchronous characteristics of these relationships.

515 *4.1. Comparison of approaches*

516 A unique feature of this study is the use of multiple statistical approaches, ranging from
517 simple (linear correlation) to more complex (GAM, IR, RF), to investigate if our understanding
518 of the predictor FCH4 relationships are influenced by the method of analysis. All statistical
519 approaches generally converged on the top predictors of FCH4 across sites and time scales
520 (Table 3). However, when considering patterns and clustering across sites, there were some
521 differences between approaches, most notably at the multiday scale (Fig. S9). For example, at the
522 multiday scale, linear correlation did not identify WTD among the top predictors (Fig. S9). The
523 lack of agreement between linear correlation and IR is similar to a previous study that combined
524 wavelet analysis and IR to investigate site-level FCH4 (Sturtevant et al., 2016). They found that,
525 while linear correlation analysis was generally capable of capturing the major diel and seasonal
526 relationships, multiday and asynchronous relationships were unresolved using linear correlation
527 (Sturtevant et al., 2016). Therefore, more complex approaches such as IR, GAM and RF may be
528 better suited for investigating complex CH_4 dynamics in wetlands.

529 *4.2. Dynamics of CH_4 exchange and influence of temperature on FCH4*

530 As observed previously (Knox et al., 2019; Sturtevant et al., 2016), the seasonal time
531 scale tended to dominate FCH4 variability across sites. The notable exceptions were some
532 tropical and subtropical sites which is expected since they typically do not experience the large

seasonal variations in temperature, radiation, and GPP that contribute to the FCH4 seasonality observed at higher latitude sites (Delwiche et al., in review).

Across all statistical methods, temperature (TS or TA) was a dominant predictor of FCH4 at the seasonal scale (Table 3, Fig. 8). This finding agrees with other studies across a range of temperate and boreal wetland ecosystems that identified TS as the dominant control over wetland FCH4 (Sachs et al., 2008; Chu et al., 2014; Turetsky et al., 2014; Knox et al., 2019; Morin, 2019). This relationship is expected because microbial activity is stimulated by increased temperature when there is no water limitation and the seasonal temperature variation is relatively large (Table 1) (Yvon-Durocher et al., 2014). However, the dominance of temperature as a driver of seasonal FCH4 in this study and earlier studies is influenced by the bias of a larger number of sites located at higher latitudes which exhibit a distinct seasonal pattern in temperature. As discussed below, FCH4 in seasonally-inundated wetlands, particularly those at lower latitudes with relatively uniform year-round temperature, were strongly influenced by WTD (Fig. 3, Fig. 4).

Across sites, lags between FCH4 and temperature at the seasonal scale were predominantly positive, with a median lag of 8 ± 16 days for TA and 5 ± 15 days for TS (Fig. 5, Fig. 8). These positive lags are generally consistent with results from a synthesis of FCH4 seasonality in freshwater wetlands of the FLUXNET-CH4 dataset that found the spring onset of FCH4 lags the increase in TS by an average of 31 ± 40 days (Delwiche et al., in review). However, the shorter median lags in this study can be explained by the fact that there was a wider range in lags observed in the FLUXNET-CH4 dataset (Delwiche et al., in review). Moreover, the lags in this study reflect the alignment between the FCH4 and TS seasonal wavelet detail which resulted in the highest IR (i.e., the lag reflects the best alignment of the

556 variability in the two timeseries and therefore greatest statistical dependence), rather than reflect
557 the numbers of days FCH4 lagged the spring increase in temperature. In the fewer instances
558 where we did observe negative lags between FCH4 and temperature, FCH4 peaked slightly
559 before TS or TA. This is also consistent with the findings of Delwiche et al. (in review) who
560 observed that for 36% of the wetland sites in the FLUXNET-CH4 database, the timing of peak
561 seasonal FCH4 led the soil temperature peak, and the findings of (Chang et al., 2021) who
562 observed a negative seasonal FCH4 hysteresis with temperature (for both the shallowest and
563 deepest TS used) at a number of sites. However, as discussed in Section 4.6, further research is
564 needed to better mechanistically constrain the causes of the observed lags, in particular for
565 factors affecting CH_4 production, oxidation, and transport (Chang et al., 2019).
566 Across multiple sites, including a range of wetland types, temperature was also a
567 dominant predictor at the multiday scale, with synoptic variations in temperature coinciding with
568 near-synchronous fluctuations in FCH4 (Fig. 6, Fig. 8). While this pattern can be in part related
569 to changes in CH_4 production with temperature (Yvon-Durocher et al., 2014), changes in
570 temperature can also influence ebullition rates and diffusive fluxes in wetlands through changes
571 in CH_4 solubility, thermal expansion and contraction of free-phase gas, and the transfer of gas
572 across the air-water interface (Table 1) (Barber et al., 1988; Chanton et al., 1989; Fechner-Levy
573 & Hemond, 1996; McNicol et al., 2017).
574 *4.3. Influence of water table dynamics on CH_4 exchange*
575 Coupling wavelet analysis with IR identified nonlinear responses of FCH4 to WTD
576 across multiple time scales (Fig.8). At the seasonal scale, WTD was the dominant driver of
577 FCH4 in wetland types and regions with pronounced seasonal variations in WTD and lower
578 variations in temperature (e.g., in seasonal wetlands and rice paddies; Bansal et al. 2018; Runkle

et al. 2019) (Fig. 3, Fig. 4). For sites where WTD was a major predictor at the seasonal scale, FCH4 lagged WTD on the order of 17 ± 11 days (Fig. 5). Lags reported here are within the range reported by other studies that found that FCH4 lagged WTD by approximately 10-11 days (Moore & Dalva, 1993; Schäfer et al., 2014; Goodrich et al., 2015). Water table fluctuations also modulated FCH4 at shorter time scales (Fig. 4). Notably, sites with fluctuating water levels tended to show pulses in FCH4 coinciding or occurring slightly before minimums in WTD, followed by a recovery in FCH4 with a lag of ~4-6 days following rising water levels (Fig. 6). This result is similar to other studies which have also found FCH4 pulses during water table drawdown (Moore & Dalva, 1993; Hatala et al., 2012b; Knox et al., 2016; Sturtevant et al., 2016; Bansal et al., 2020). These interactions are consistent with the release of stored CH_4 as hydrostatic pressure drops, with peak release occurring as the water table crosses the soil surface (Knox et al., 2016; Chen et al., 2017; Ueyama et al., 2020b). As illustrated in Fig. 6f, different magnitudes of FCH4 pulses are therefore likely dependent on the current CH_4 pool in porewater and CH_4 production rates (Sturtevant et al., 2016; Bansal et al., 2020). Furthermore, sustained reduction in FCH4 following rises in water levels likely result from the time taken to deplete reoxidized alternative electron acceptors or replenish the soil CH_4 pool, causing a slow return to higher CH_4 fluxes (Moore & Dalva, 1993; Sturtevant et al., 2016; Koebsch et al., 2020a). This mechanism can also explain the delay in the rise in FCH4 following the rise in WTD at the seasonal scale, which is consistent with studies that show recovery time of FCH4 from weeks to months following re-wetting (Table 1) (Kim et al., 2012).

While saturated conditions are generally a prerequisite for CH_4 production (Bridgham et al., 2013), although not exclusively (Angle et al., 2017), WTD did not appear as an important predictor for sites exhibiting relatively low variation in WTD (Fig. 4). This is similar to other

602 studies of wetland CH_4 exchange where the water table remained above the surface or showed
603 little variation (Song et al., 2011; Strachan et al., 2015; Knox et al., 2016; Yang et al., 2017).
604 This result highlights the limitation of these types of observational studies to identify controls
605 that do not vary, and underscores the need for experimental studies and long-term continuous
606 measurements of ecosystem-scale FCH4 to capture a wide range of environmental conditions
607 (Sturtevant et al., 2016).

608 *4.4. Role of pressure fluctuations on CH_4 exchange*

609 Atmospheric pressure is often observed to be an important control on FCH4 from
610 peatlands, with ebullition being the main transport mechanisms during the pressure-falling phase
611 (Table 1) (Tokida, 2005; Tokida et al., 2007; Sachs et al., 2008; Nadeau et al., 2013). Decreasing
612 PA can lead to gas release from solution and the enlargement of the volume of gas, resulting in
613 increased ebullition (Tokida et al., 2007). Similarly, in freshwater lake environments, a
614 correlation between low PA and increased rates of FCH4 is frequently observed (Mattson &
615 Likens, 1990; Casper et al., 2000; Engle & Melack, 2000). We found that PA was a dominant
616 predictor on FCH4 in several peat dominated sites across a range of wetland types (Fig. 4, Fig.
617 8). As in other studies (Nadeau et al., 2013), we found that drops in PA coincided with
618 synchronous releases of CH_4, with synoptic variations in PA resulting in CH_4 pulses on the order
619 of 5 to 100 nmol m^{-2} s^{-1} (Fig. S10).

620 *4.5. Influence of plant activity on FCH4 and the relationship between LE and FCH4*

621 At the seasonal scale, LE, GPP and NEE were generally found to be secondary predictors
622 of FCH4 (Table 3, Fig. 8). While LE does not directly drive FCH4, the few studies that have
623 examined the relationship between FCH4 and LE have always found it to be significant (Morin
624 et al., 2014; Sturtevant et al., 2016; Morin, 2019). This strong association between LE and FCH4

625 is due to the fact that evaporation of water and CH_4 volatilization from water and plant surfaces
626 are driven by similar physical mechanisms and therefore tend to covary (Table 1) (Morin, 2019).
627 LE is also linked to plant activity (e.g., Leaf Area Index (LAI) is a strong determinant of LE) at
628 the seasonal scale, and hence LE can represent a proxy for CH_4 transport through
629 aerenchymatous vegetation (Table 1) (Morin et al., 2014; Morin, 2019).
630 GPP represents a proxy for the mechanisms of carbon inputs and root exudates to fuel
631 methanogenesis, plant-mediated transport of CH_4 to the atmosphere via aerenchymatous tissue,
632 and oxygen transport via aerenchyma into the soil fuel methane oxidation and/or reduce methane
633 production (Table 1) (Turetsky et al., 2014). The first two mechanisms increase FCH4 while the
634 latter decrease FCH4. Similar to other studies (Chu et al., 2014; Morin et al., 2014; Rinne et al.,
635 2018), GPP was found to be among the top predictors of FCH4 at the seasonal scale across
636 multiple sites, although it always followed temperature in relative importance (Fig. 3, Fig. S3).
637 The relationship between GPP and FCH4 observed in this study supports earlier studies
638 suggesting that the relationship between GPP and FCH4 is dominated by either the addition of
639 root exudates to the rhizosphere, particularly for deeper rooted plants, or the result of increased
640 CH_4 transport through aerenchymatous vegetation (Bellisario et al., 1999; Hargreaves et al.,
641 2001; Hatala et al., 2012a; Chu et al., 2014)
642 At the seasonal scale, FCH4 lagged both LE (17 ± 18 days) and GPP (~13 ± 23 days)
643 considerably. These lags reflect the fact that GPP and LE peaked before FCH4, similar to the
644 findings of Delwiche et al. (in review) and Mitra et al. (2020). At the seasonal scale, this lag
645 suggests a delay between labile organic carbon inputs from plants (either in the form of exudates
646 or fresh detritus) and FCH4 (Megonigal et al., 2004). Alternatively, this delay could be caused
647 by confounding variables such as temperature (Rinne et al., 2018), again highlighting the

importance of considering direct drivers of CH_4 production, oxidation and transport (e.g., substrate availability, microbial composition, redox) rather than proxies (e.g., GPP) for these controls as we were limited to in this study.

As observed in other studies, plant activity was linked to FCH4 at the diel scale (Table 3, Fig. 3, Fig. 8). While studies generally agree that plant activity controls diel variations in wetland FCH4, it is challenging to identify whether the direct mechanism is the strength of internal gas transport, stomatal conductance, or stimulation of CH_4 production through a supply of photosynthate as root exudates (Van der Nat & Middelburg, 2000; Hatala et al., 2012a; Morin et al., 2014; Koebsch et al., 2015). Our observation that LE and VPD were generally the strongest synchronous diel predictors of FCH4 suggests that internal gas transport rather than stomatal conductance (as represented by synchronous coupling between FCH4 and GPP, NEE or SW_IN) generally controls FCH4 at the diel scale (Table 1) (Sturtevant et al., 2016; Villa et al., 2020). If we consider maximum IR at the diel scale, lags with LE and VPD were small, again supporting the role of VPD-pressurized ventilation mechanism as an important mechanism driving CH_4 exchange in these sites with aerenchymatous vegetation (Table 1, Table 2). The strong co-variance of FCH4 with LE and VPD also suggests that the physical processes that control evaporation and boundary layer mixing exert very similar controls on CH_4 volatilization (Table 1). At four sites, maximum IR was between GPP or NEP and FCH4, suggesting that recent photosynthates may also control FCH4 at the diel scale (Table 1), with a lag on the order of 1 to 4 hours (Fig. 8). These lags are comparable to other studies which found that GPP caused a diurnal pattern in CH_4 emissions (Hatala et al., 2012a; Knox et al., 2016, Mitra et al. 2020). However, in some cases where GPP was identified as a dominant predictor of FCH4 at the diel

scale, GPP seemed to modulate the amplitude of the diel pattern rather than the shape of the diel pattern in FCH4 (Fig. S11).

4.6. Limitations and next steps

Though separating the time scales of variation was useful for isolating and identifying dominant predictors of FCH4, one limitation of these approaches is that they do not explicitly account for dependencies and interactions among drivers (Sturtevant et al., 2016). For example, temperature may be a confounding effect when interpreting the importance of LE and GPP at the seasonal scale since temperature influences both of these variables. Similarly, RF variable importance rankings can be susceptible to shuffling when highly correlated predictors are present, though this was not observed in this study. While in this study we assume that a stronger variable importance metric provides evidence that a given predictor is more important, future work could explicitly consider partial or interactive effects among drivers. For instance, future studies could test approaches such as conditional or partial mutual information (Frenzel & Pompe, 2007; Sharma & Mehrotra, 2014; Zhao et al., 2016), conditional variable importance for RF (Strobl et al., 2008), or commonality analysis and structural equation modeling (Koebsch, Sonnentag, et al., 2020) to characterize interactions and interdependencies among multiple predictors.

Additionally, future research could focus on addressing causation in a similar nonlinear, multiresolution framework. While the methods selected here were used due to their widespread application and intuitive statistical interpretation, other methods are better suited for assessing causation (Runge et al. 2019). For instance, Granger causality has been used for assigning causation in environmental time series (Molini et al., 2010; Detto et al., 2012; Hatala et al., 2012a). Transfer entropy, which quantifies information flow rather than simply overlap, is a

693 nonparametric information theory metric that implies causation (Schreiber, 2000). Here, we
694 focused on mutual information over transfer entropy due to its lower data requirements (Ruddell
695 & Kumar, 2009) and greater ease of interpretation (Sturtevant et al., 2016). However, future
696 work could focus on more explicitly addressing causation.

697 While 42 freshwater wetland sites are currently included in the FLUXNET-CH4 dataset
698 (Delwiche et al., in review), the lack of ancillary measurements (most notably WTD) precluded
699 the inclusion of many sites from our analysis. Furthermore, the dataset contains far fewer sites in
700 the tropics relative to higher latitude regions (Delwiche et al., in review). As such, our analysis is
701 limited to a subset of 23 sites, predominantly located in temperate and boreal latitudes (Fig. 1).
702 The inclusion of a handful of subtropical and tropical sites in this study highlights the differences
703 in the dominant predictors of FCH4 at the seasonal scale between low latitude, seasonal wetlands
704 and higher latitude sites (i.e., the relative importance of WTD vs. temperature). Moving forward,
705 we encourage site principal investigators to measure and report the full suite of variables listed in
706 Table 1 and to expand the number of low latitude sites so that future studies can include a larger
707 number of sites with greater spatial coverage in the tropics. This expansion can improve the
708 spatial representativeness of sites in future analyses ensuring that our understanding of wetland
709 FCH4 does not remain biased towards temperate and high latitude regions, particularly in North
710 America and Europe (Fig. 1). It can also increase the statistical power of future studies.

711 Finally, while coupling wavelet decomposition and the statistical analyses presented here
712 provides a valuable post hoc tool for inferring controls on FCH4 and can generally explain much
713 of the variability in FCH4 across scales, they are empirical approaches focused on net FCH4, and
714 therefore do not explicitly allow for direct assessment of the drivers of CH_4 production,
715 oxidation, and transport (Table 1). As mentioned above, future work could focus on better

integrating eddy covariance FCH4 measurements across sites with critical but often missing drivers of FCH4. For instance, this includes direct measurements of redox potential and oxygen content, substrate availability, and detailed information on soil microbial communities driving CH_4 production and consumption (Kwon et al., 2017; Nemitz et al., 2018). Furthermore, this could be done in a spatially explicit manner to better understand site-level heterogeneity, which is something that was not directly addressed in this study due to the integrative nature of eddy covariance measurements (although we did explore site-level heterogeneity to some extent by including wind direction, but these variables did not come up as dominant variables in the analyses). Future research should also focus on pairing eddy covariance observations with stable isotope analyses of CH_4, and incubation, chamber, and leaf level measurements to provide improved understanding of the direct mechanisms of CH_4 production, transport and oxidation (Chanton et al., 1997; Marushchak et al., 2016; Villa et al., 2020). In particular, with respect to CH_4 transport and controls on FCH4 at the diel scale, given that the majority of the sites measured FCH4 using an open-path sensor, it is also possible that density corrections may have influenced diel patterns in CH_4 exchange, and in turn the evaluation of biophysical predictors of FCH4 and associated lags (Chamberlain et al., 2017). As such, coupling eddy covariance measurements with leaf chamber measurements or isotope analyses is especially useful for better identifying controls on diel scale FCH4.

Nonetheless, by combining multiple statistical methods in a wavelet-based multi-resolution framework, this study contributes to an improved understanding of the predictors of FCH4 across a wide range of non-tidal, freshwater wetlands, which can help inform empirical and process-based models of FCH4 (Oikawa et al., 2017). As such, while our analysis does not provide an explicit predictive model, it does provide the timing and scale-dependent information

739 that can help guide modeling efforts toward better representing scale-dependent, asynchronous
740 and nonlinear processes inherent in FCH4 (Sturtevant et al., 2016), thereby helping better
741 constrain wetland CH_4 emissions.

742 **5. Acknowledgements**
743
744 We acknowledge primary support from the Gordon and Betty Moore Foundation (Grant
745 GBMF5439, "Advancing Understanding of the Global Methane Cycle"; Stanford University)
746 and from the John Wesley Powell Center for Analysis and Synthesis of the U.S. Geological
747 Survey ("Wetland FLUXNET Synthesis for Methane" working group). Benjamin R. K. Runkle
748 was supported by the National Science Foundation (NSF) Award 1752083. Masahito Ueyama
749 was supported by ArCS II (JPMXD1420318865) and JSPS KAKENHI (20K21849). William J.
750 Riley and Qing Zhu were supported by the U.S. Department of Energy (DOE) BER-RGCM-
751 RUBISCO project (DEAC02-05CH11231). Jessica Turner acknowledges support from NSF
752 GRFP (DGE-1747503) and NTL LTER (DEB-1440297). Minseok Kang was supported by the
753 National Research Foundation of Korea (NRF-2018 R1C1B6002917). Rodrigo Vargas
754 acknowledges support from NSF (grant #1652594). Dennis Baldocchi acknowledges the
755 California Department of Water Resources for a funding contract from the California
756 Department of Fish and Wildlife and the U.S. Department of Agriculture (NIFA grant #2011-
757 67003-30371). Oliver Sonnentag acknowledges funding by the Canada Research Chairs, Canada
758 Foundation for Innovation Leaders Opportunity Fund, and Natural Sciences and Engineering
759 Research Council Discovery Grant Programs for work at CA-SCB. Benjamin Poulter
760 acknowledges support from the NASA Carbon Cycle and Ecosystems Program. Gil Bohrer
761 acknowledges funding by DOE (DE-SC0021067) and the Ohio Department of Natural Resources
762 (Subaward N18B 315-11). Pavel Alekseychik acknowledges support from the CLIMOSS project

763 funded by the Academy of Finland (grant #296116), and the SOMPA project funded by the
764 Strategic Research Council at the Academy of Finland (grant #312912). Tuula Aalto and
765 Annalea Lohila acknowledge the support from the Academy of Finland project UPFORMET
766 (grant #307331). Eeva-Stiina Tuittila acknowledges support from the Academy of Finland
767 (grants #287039 and #330840). Mats Nilsson and Matthias Peichl acknowledge support from the
768 Swedish national research infrastructure ICOS and SITES and from the Swedish Research
769 Council, Swedish Research Council for Environment, Agricultural Sciences and Spatial Planning
770 and the Kempe Foundation. Pia Gottschalk acknowledges support from the German Federal
771 Ministry of Food and Agriculture (BMEL) within the ERA-NET FACCE ERA-GAS, with
772 FACCE ERA-GAS received funding from the European Union's Horizon 2020 Research and
773 Innovation Programme (grant #696356). The FI-Lom, FI-Sii, and SE-Deg sites are part of the
774 ICOS European Research Infrastructure. We acknowledge the following AmeriFlux sites for
775 their data records: US-Uaf, US-Los, US-Myb, US-OWC, US-Tw1, US-Tw4, US-WPT, US-
776 MAC. In addition, funding for AmeriFlux data resources and core site data was provided by the
777 DOE's Office of Science.
778
779
780

781 **References**

782 Abdi, H., & Williams, L. J. (2010). Principal component analysis. *Wiley Interdisciplinary*
783 *Reviews: Computational Statistics, 2*(4), 433–459. https://doi.org/10.1002/wics.101.
784 Angle, J. C., Morin, T. H., Solden, L. M., Narrowe, A. B., Smith, G. J., Borton, M. A., Rey-
785 Sanchez, C., Daly, R. A., Mirfenderesgi, G., Hoyt, D. W., Riley, W. J., Miller, C. S., Bohrer,
786 G., & Wrighton, K. C. (2017). Methanogenesis in oxygenated soils is a substantial fraction
787 of wetland methane emissions. *Nature Communications, 8*(1567).
788 https://doi.org/10.1038/s41467-017-01753-4.
789 Aurela, M., Lohila, A. Tuovinen, J.-P., Hatakka, J., Rainne, J., Mäkelä, T., and Lauria, T.
790 (2020). FLUXNET-CH4 FI-Lom Lompolojankka. Finland.
791 https://doi:10.18140/FLX/1669638.
792 Baldocchi, D. (2014). Measuring fluxes of trace gases and energy between ecosystems and the
793 atmosphere - the state and future of the eddy covariance method. *Global Change Biology*,
794 *20*(12), 3600–3609. https://doi.org/10.1111/gcb.12649.
795 Bansal, S., Tangen, B., & Finocchiaro, R. (2018). Diurnal patterns of methane flux from a
796 seasonal wetland: mechanisms and methodology. Wetlands, 38(5), 933–943.
797 https://doi.org/10.1007/s13157-018-1042-5.
798 Bansal, S., Johnson, O. F., Meier, J., & Zhu, X. (2020). Vegetation affects timing and location of
799 wetland methane emissions. *Journal of Geophysical Research: Biogeosciences, 125,*
800 e2020JG00577. https://doi.org/10.1029/2020JG005777.
801 Barber, T. R., Burke, R. A., Jr., & Sackett, W. M. (1988). Diffusive flux of methane from warm
802 wetlands. *Global Biogeochemical Cycles, 2*(4), 411–425.
803 https://doi.org/10.1029/GB002i004p00411.

804 Bellisario, L. M., Bubier, J. L., Moore, T. R., & Chanton, J. P. (1999). Controls on CH_4
805 emissions from a northern peatland. *Global Biogeochemical Cycles, 13*(1), 81–91.
806 https://doi.org/10.1029/1998GB900021.
807 Bohrer, G., Kerns, J., Morin, T.H., Rey-Sanchez, A.C., Villa, J., and Ju, Y. (2020). FLUXNET-
808 CH4 US-OWC Old Woman Creek. United States. https://doi:10.18140/FLX/1669690.
809 Breiman, L. (2001). Random Forests. *Machine Learning, 45*(1), 5–32.
810 https://doi.org/10.1023/A:1010933404324.
811 Bridgham, S. D., Cadillo-Quiroz, H., Keller, J. K., & Zhuang, Q. (2013). Methane emissions
812 from wetlands: biogeochemical, microbial, and modeling perspectives from local to global
813 scales. *Global Change Biology, 19*(5), 1325–1346. https://doi.org/10.1111/gcb.12131.
814 Bubier, J. L., Moore, T. R., Bellisario, L., Comer, N. T., & Crill, P. M. (1995). Ecological
815 controls on methane emissions from a northern peatland complex in the zone of
816 discontinuous permafrost, Manitoba, Canada. *Global Biogeochemical Cycles, 9*(4), 455–
817 470. https://doi.org/10.1029/95gb02379.
818 Campbell, D., and Goodrich, J. (2020). FLUXNET-CH4 NZ-Kop Kopuatai. New Zealand.
819 https://doi:10.18140/FLX/1669652.
820 Casper, P., Maberly, S. C., Hall, G. H., & Finlay, B. J. (2000). Fluxes of methane and carbon
821 dioxide from a small productive lake to the atmosphere. *Biogeochemistry, 49*(1), 1–19.
822 https://doi.org/10.1023/A:1006269900174.
823 Chamberlain, S. D., Verfaillie, J., Eichelmann, E., Hemes, K. S., & Baldocchi, D. D. (2017).
824 Evaluation of density corrections to methane fluxes measured by open-path eddy covariance
825 over contrasting landscapes. *Boundary-Layer Meteorology, 165*(2), 197–210.
826 https://doi.org/10.1007/s10546-017-0275-9.

827 Chang, K., Riley, W. J., Brodie, E. L., McCalley, C. K., Crill, P. M., & Grant, R. F. (2019).
828 Methane production pathway regulated proximally by substrate availability and distally by
829 temperature in a high-latitude mire complex. *Journal of Geophysical Research:*
830 *Biogeosciences, 124*(10), 3057–3074. https://doi.org/10.1029/2019JG005355.
831 Chang, K. Y., W. J. Riley, S. H. Knox, R. B. Jackson, G. McNicol, B. Poulter, M. Aurela, D.
832 Baldocchi, S. Bansal, G. Bohrer, D. I. Campbell, A. Cescatti, H. Chu, K. B. Delwiche, A.
833 Desai, E. Euskirchen, T. Friborg, M. Goeckede, G. Holm, M. Kang, T. Keenan, K. W.
834 Krauss, A. Lohila, I. Mammarella, A. Miyata, & Others (2021). Global wetland methane
835 emissions have hysteretic responses to seasonal temperature. *Nature Communications*, 12,
836 2266, https://doi.org/10.1038/s41467-021-22452-1.
837 Chanton, J. P., Martens, C. S., & Kelley, C. A. (1989). Gas transport from methane-saturated,
838 tidal freshwater and wetland sediments. *Limnology and Oceanography, 34*(5), 807–819.
839 https://doi.org/10.4319/lo.1989.34.5.0807.
840 Chanton, J. P., Whiting, G. J., Blair, N. E., Lindau, C. W., & Bollich, P. K. (1997). Methane
841 emission from rice: Stable isotopes, diurnal variations, and CO_2 exchange. *Global*
842 *Biogeochemical Cycles, 11*(1), 15–27. https://doi.org/10.1029/96GB03761.
843 Chen, J., and Housen Chu. (2020). FLUXNET-CH4 US-WPT Winous Point North Marsh.
844 United States. doi:10.18140/FLX/1669702.
845 Chen, W., Zhang, F., Wang, B., Wang, J., Tian, D., Han, G., Wen, X., Yu, G., & Niu, S. (2019).
846 Diel and seasonal dynamics of ecosystem-scale methane flux and their determinants in an
847 alpine meadow. *Journal of Geophysical Research: Biogeosciences, 124*(6), 1731–1745.
848 https://doi.org/10.1029/2019jg005011.

849 Chen, X., Schäfer, K. V. R., & Slater, L. (2017). Methane emission through ebullition from an
850 estuarine mudflat: 2. Field observations and modeling of occurrence probability. *Water*
851 *Resources Research, 53*(8), 6439–6453. https://doi.org/10.1002/2016wr019720.
852 Christensen, T. R., Ekberg, A., Ström, L., Mastepanov, M., Panikov, N., Öquist, M., Svensson,
853 B. H., Nykänen, H., Martikainen, P. J., & Oskarsson, H. (2003). Factors controlling large
854 scale variations in methane emissions from wetlands. *Geophysical Research Letters, 30*(7),
855 261. https://doi.org/10.1029/2002GL016848.
856 Chu, H., Chen, J., Gottgens, J. F., Ouyang, Z., John, R., Czajkowski, K., & Becker, R. (2014).
857 Net ecosystem methane and carbon dioxide exchanges in a Lake Erie coastal marsh and a
858 nearby cropland. *Journal of Geophysical Research: Biogeosciences, 119*(5), 722–740.
859 https://doi.org/10.1002/2013JG002520.
860 Cornish, C. R., D. B. Percival, and C. S. Bretherton (2003). The WMTSA Wavelet Toolkit for
861 data analysis in the geosciences. Eos Trans. AGU, 84(46), Fall Meet. Suppl., Abstract
862 NG11A-0173.
863 Delwiche, K. B., Knox, S. H., Malhotra, A., Fluet-Chouinard, E., McNicol, G., Feron, S.,
864 Ouyang, Z., Papale, D., Trotta, C., Canfora, E., Chea, Y.-W., Christianson, D., Alberto, M.
865 C. R., Alekseychik, P., Aurela, M. & Others. (In Review). FLUXNET-CH4: A global,
866 multi-ecosystem dataset and analysis of methane seasonality from freshwater wetlands.
867 *Earth System Science Data.*
868 Desai, A. R., Xu, K., Tian, H., Weishampel, P., Thom, J., Baumann, D., Andrews, A. E., Cook,
869 B. D., King, J. Y., & Kolka, R. (2015). Landscape-level terrestrial methane flux observed
870 from a very tall tower. *Agricultural and Forest Meteorology, 201,* 61–75.
871 https://doi.org/10.1016/j.agrformet.2014.10.017.

872 Desai, A. R., and Thom, J. (2020). FLUXNET-CH4 US-Los Lost Creek. United States.
873 https://doi:10.18140/FLX/1669682.
874 Detto, M., Molini, A., Katul, G., Stoy, P., Palmroth, S., & Baldocchi, D. (2012). Causality and
875 persistence in ecological systems: a nonparametric spectral granger causality approach. *The*
876 *American Naturalist, 179*(4), 524–535. https://doi.org/10.1086/664628.
877 Eichelmann, E., Knox, S., Rey-Sanchez, A.C, Valach, A., Sturtevant, C., Szutu, D., Verfaillie, J.,
878 and Baldocchi, D. (2020). FLUXNET-CH4 US-Tw4 Twitchell East End Wetland. United
879 States. https://doi:10.18140/FLX/1669698.
880 Engle, D., & Melack, J. M. (2000). Methane emissions from an Amazon floodplain lake:
881 Enhanced release during episodic mixing and during falling water. *Biogeochemistry, 51*(1),
882 71–90. https://doi.org/10.1023/A:1006389124823.
883 Etminan, M., Myhre, G., Highwood, E. J., & Shine, K. P. (2016). Radiative forcing of carbon
884 dioxide, methane, and nitrous oxide: A significant revision of the methane radiative forcing.
885 *Geophysical Research Letters, 43*(24), 12,614–12,623.
886 https://doi.org/10.1002/2016gl071930.
887 Fechner-Levy, E. J., & Hemond, H. F. (1996). Trapped methane volume and potential effects on
888 methane ebullition in a northern peatland. *Limnology and Oceanography, 41*(7), 1375–1383.
889 https://doi.org/10.4319/lo.1996.41.7.1375.
890 Fraser, A. M., & Swinney, H. L. (1986). Independent coordinates for strange attractors from
891 mutual information. *Physical Review A: General Physics, 33*(2), 1134–1140.
892 https://doi.org/10.1103/physreva.33.1134.

893 Frenzel, S., & Pompe, B. (2007). Partial mutual information for coupling analysis of multivariate
894 time series. *Physical Review Letters, 99*(20), 204101.
895 https://doi.org/10.1103/PhysRevLett.99.204101.
896 Genuer, R., Poggi, J.-M., & Tuleau-Malot, C. (2010). Variable selection using random forests.
897 *Pattern Recognition Letters, 31*(14), 2225–2236.
898 https://doi.org/10.1016/j.patrec.2010.03.014.
899 Goodrich, J. P., Campbell, D. I., Roulet, N. T., Clearwater, M. J., & Schipper, L. A. (2015).
900 Overriding control of methane flux temporal variability by water table dynamics in a
901 Southern Hemisphere, raised bog. *Journal of Geophysical Research: Biogeosciences,*
902 *120*(5), 819–831. https://doi.org/10.1002/2014JG002844.
903 Gregory R. Warnes, Ben Bolker, Lodewijk Bonebakker, Robert Gentleman, Wolfgang Huber
904 Andy Liaw, Thomas Lumley, Martin Maechler, Arni Magnusson, Steffen Moeller, Marc
905 Schwartz and Bill Venables. (2019). gplots: Various R programming tools for plotting data.
906 https://cran.r-project.org/web/packages/gplots/index.html.
907 Hargreaves, K. J., Fowler, D., Pitcairn, C. E. R., & Aurela, M. (2001). Annual methane emission
908 from Finnish mires estimated from eddy covariance campaign measurements. *Theoretical*
909 *and Applied Climatology, 70*(1), 203–213. https://doi.org/10.1007/s007040170015.
910 Hatala, J. A., Detto, M., & Baldocchi, D. D. (2012a). Gross ecosystem photosynthesis causes a
911 diurnal pattern in methane emission from rice. *Geophysical Research Letters, 39*(6).
912 https://doi.org/10.1029/2012GL051303.
913 Hatala, J. A., Detto, M., Sonnentag, O., Deverel, S. J., Verfaillie, J., & Baldocchi, D. D. (2012b).
914 Greenhouse gas (CO_2, CH_4, H_2O) fluxes from drained and flooded agricultural peatlands in

the Sacramento-San Joaquin Delta. *Agriculture, Ecosystems & Environment, 150*, 1–18. https://doi.org/10.1016/j.agee.2012.01.009.

Hollinger, D. Y., & Richardson, A. D. (2005). Uncertainty in eddy covariance measurements and its application to physiological models. *Tree Physiology, 25*(7), 873–885. https://doi.org/10.1093/treephys/25.7.873.

Iwata, H. (2020a). FLUXNET-CH4 JP-Mse Mase rice paddy field. Japan. https://doi:10.18140/FLX/1669647.

Iwata, H., Ueyama M., and Harazono, Y. (2020b). FLUXNET-CH4 US-Uaf University of Alaska, Fairbanks. United States. Web. https://doi:10.18140/FLX/1669701.

Jackson, R. B., Saunois, M., Bousquet, P., Canadell, J. G., Poulter, B., Stavert, A. R., Bergamaschi, P., Niwa, Y., Segers, A., & Tsuruta, A. (2020). Increasing anthropogenic methane emissions arise equally from agricultural and fossil fuel sources. *Environmental Research Letters, 15,* 071002. https://doi.org/10.1088/1748-9326/ab9ed2.

Jammet, M., Dengel, S., Kettner, E., Parmentier, F.-J. W., Wik, M., Crill, P., & Friborg, T. (2017). Year-round CH_4 and CO_2 flux dynamics in two contrasting freshwater ecosystems of the subarctic. *Biogeosciences, 14*(22), 5189–5216. https://doi.org/10.5194/bg-14-5189-2017.

Kim, D.-G., Vargas, R., Bond-Lamberty, B., & Turetsky, M. R. (2012). Effects of soil rewetting and thawing on soil gas fluxes: a review of current literature and suggestions for future research. *Biogeosciences, 9(*7), 2459–2483. https://doi.org/10.5194/bg-9-2459-2012.

Kim, Y., Johnson, M. S., Knox, S. H., Andrew Black, T., Dalmagro, H. J., Kang, M., Kim, J., & Baldocchi, D. (2020). Gap-filling approaches for eddy covariance methane fluxes: A comparison of three machine learning algorithms and a traditional method with principal

component analysis. *Global Change Biology, 26*(3), 1499–1518. https://doi.org/10.1111/gcb.14845.

Knoblauch, C., Spott, O., Evgrafova, S., Kutzbach, L., & Pfeiffer, E. (2015). Regulation of methane production, oxidation, and emission by vascular plants and bryophytes in ponds of the northeast Siberian polygonal tundra. *Journal of Geophysical Research: Biogeosciences, 120*(12), 2525–2541. https://doi.org/10.1002/2015JG003053.

Knox, S. H., Matthes, J. H., Sturtevant, C., Oikawa, P. Y., Verfaillie, J., & Baldocchi, D. (2016). Biophysical controls on interannual variability in ecosystem-scale CO_2 and CH_4 exchange in a California rice paddy. *Journal of Geophysical Research: Biogeosciences, 121*(3), 978–1001. https://doi.org/10.1002/2015JG003247.

Knox, S. H., Jackson, R. B., Poulter, B., McNicol, G., Fluet-Chouinard, E., Zhang, Z., Hugelius, G., Bousquet, P., Canadell, J. G., Saunois, M., Papale, D., Chu, H., Keenan, T. F., Baldocchi, D., Torn, M. S., Mammarella, I., Trotta, C., Aurela, M., Bohrer, G., & Others. (2019). FLUXNET-CH4 synthesis activity: objectives, observations, and future directions. *Bulletin of the American Meteorological Society, 100*(12), 2607–2632. https://doi.org/10.1175/BAMS-D-18-0268.1.

Knox, Sara, Matthes, J. H., Verfaillie, J., and Baldocchi, D. (2020). FLUXNET-CH4 US-Twt Twitchell Island. United States, (2020). Web. https://doi:10.18140/FLX/1669700.

Koebsch, F., Jurasinski, G., Koch, M., Hofmann, J., & Glatzel, S. (2015). Controls for multi-scale temporal variation in ecosystem methane exchange during the growing season of a permanently inundated fen. *Agricultural and Forest Meteorology, 204,* 94–105. https://doi.org/10.1016/j.agrformet.2015.02.002.

959 Koebsch, F., Gottschalk, P., Beyer, F., Wille, C., Jurasinski, G., & Sachs, T. (2020a). The impact
960 of occasional drought periods on vegetation spread and greenhouse gas exchange in
961 rewetted fens. *Philosophical Transactions of the Royal Society of London, Series B,*
962 *Biological Sciences, 375*(1810), 20190685. https://doi.org/10.1098/rstb.2019.0685.
963 Koebsch, F., and Jurasinski, G. (2020b). FLUXNET-CH4 DE-Hte Huetelmoor. Germany.
964 https://doi:10.18140/FLX/1669634.
965 Koebsch, F., Sonnentag, O., Järveoja, J., Peltoniemi, M., Alekseychik, P., Aurela, M., Arslan, A.
966 N., Dinsmore, K., Gianelle, D., Helfter, C., Jackowicz-Korczynski, M., Korrensalo, A.,
967 Leith, F., Linkosalmi, M., Lohila, A., Lund, M., Maddison, M., Mammarella, I., Mander, Ü.,
968 & Others. (2020c). Refining the role of phenology in regulating gross ecosystem
969 productivity across European peatlands. *Global Change Biology, 26*(2), 876–887.
970 https://doi.org/10.1111/gcb.14905.
971 Kwon, M. J., Beulig, F., Ilie, I., Wildner, M., Küsel, K., Merbold, L., Mahecha, M. D., Zimov,
972 N., Zimov, S. A., Heimann, M., Schuur, E. A. G., Kostka, J. E., Kolle, O., Hilke, I., &
973 Göckede, M. (2017). Plants, microorganisms, and soil temperatures contribute to a decrease
974 in methane fluxes on a drained Arctic floodplain. *Global Change Biology, 23*(6), 2396–
975 2412. https://doi.org/10.1111/gcb.13558.
976 Laanbroek, H. J. (2010). Methane emission from natural wetlands: interplay between emergent
977 macrophytes and soil microbial processes. A mini-review. *Annals of Botany, 105*(1), 141–
978 153. https://doi.org/10.1093/aob/mcp201.
979 Lai, D. Y. F. (2009). Methane dynamics in northern peatlands: A review. *Pedosphere, 19*(4),
980 409–421. https://doi.org/10.1016/s1002-0160(09)00003-4.

981 Li, H., Dai, S., Ouyang, Z., Xie, X., Guo, H., Gu, C., Xiao, X., Ge, Z., Peng, C., & Zhao, B.
982 (2018). Multi-scale temporal variation of methane flux and its controls in a subtropical tidal
983 salt marsh in eastern China. *Biogeochemistry, 137*(1), 163–179.
984 https://doi.org/10.1007/s10533-017-0413-y.
985 Linkhorst, A., Hiller, C., DelSontro, T., M. Azevedo, G., Barros, N., Mendonça, R., & Sobek, S.
986 (2020). Comparing methane ebullition variability across space and time in a Brazilian
987 reservoir. *Limnology and Oceanography, 65*(7), 1623–1634.
988 https://doi.org/10.1002/lno.11410.
989 Malhotra, A., & Roulet, N. T. (2015). Environmental correlates of peatland carbon fluxes in a
990 thawing landscape: do transitional thaw stages matter? *Biogeosciences, 12*(10), 3119–3130.
991 https://doi.org/10.5194/bg-12-3119-2015.
992 Marushchak, M. E., Friborg, T., Biasi, C., Herbst, M., Johansson, T., Kiepe, I., Liimatainen, M.,
993 Lind, S. E., Martikainen, P. J., Virtanen, T., Soegaard, H., & Shurpali, N. J. (2016). Methane
994 dynamics in the subarctic tundra: combining stable isotope analyses, plot- and ecosystem-
995 scale flux measurements. *Biogeosciences, 13*(2), 597–608. https://doi.org/10.5194/bg-13-
996 597-2016.
997 Matthes, J.H., Sturtevant, C., Oikawa, P., Chamberlain, S.D., Szutu, D., Ortiz A. A., Verfaillie,
998 J., and Baldocchi, D. (2020). FLUXNET-CH4 US-Myb Mayberry Wetland. United States.
999 https://doi:10.18140/FLX/1669685.
1000 Mattson, M. D., & Likens, G. E. (1990). Air pressure and methane fluxes. *Nature, 347*(6295),
1001 718–719. https://doi.org/10.1038/347718b0.
1002 McNicol, G., Sturtevant, C. S., Knox, S. H., Dronova, I., Baldocchi, D. D., & Silver, W. L.
1003 (2017). Effects of seasonality, transport pathway, and spatial structure on greenhouse gas

1004 fluxes in a restored wetland. *Global Change Biology, 23*(7), 2768–2782.
1005 https://doi.org/10.1111/gcb.13580.
1006 Megonigal, J. P., Hines, M. E., & Visscher, P. T. (2004). Anaerobic metabolism: linkages to
1007 trace gases and aerobic processes. In Schlesinger, W., Holland, H. and Turekian, K. (Eds.),
1008 Treatise on Geochemistry (Volume 8, pp. 317-424). Elsevier.
1009 Mitra, B., Minick, K., Miao, G., Domec, J.-C., Prajapati, P., McNulty, S. G., Sun, G., King, J. S.,
1010 & Noormets, A. (2020). Spectral evidence for substrate availability rather than
1011 environmental control of methane emissions from a coastal forested wetland. Agricultural
1012 and Forest Meteorology, 291, 108062. https://doi.org/10.1016/j.agrformet.2020.108062.
1013 Molini, A., Katul, G. G., & Porporato, A. (2010). Causality across rainfall time scales revealed
1014 by continuous wavelet transforms. *Journal of Geophysical Research, 115*(D14), 579.
1015 https://doi.org/10.1029/2009JD013016.
1016 Moore, T. R., & Knowles, R. (1989). The influence of water table levels on methane and carbon
1017 dioxide emissions from peatland soils. *Canadian Journal of Soil Science, 69*(1), 33–38.
1018 https://doi.org/10.4141/cjss89-004.
1019 Moore, T. R., & Dalva, M. (1993). The influence of temperature and water table position on
1020 carbon dioxide and methane emissions from laboratory columns of peatland soils. *Journal of*
1021 *Soil Science, 44*(4), 651–664. https://doi.org/10.1111/j.1365-2389.1993.tb02330.x.
1022 Morin, T. H., Bohrer, G., Frasson, R. P. d. M., Naor-Azreli, L., Mesi, S., Stefanik, K. C., &
1023 Schäfer, K. V. R. (2014). Environmental drivers of methane fluxes from an urban temperate
1024 wetland park. *Journal of Geophysical Research: Biogeosciences, 119*(11), 2188–2208.
1025 https://doi.org/10.1002/2014JG002750.

1026 Morin, T. H. (2019). Advances in the eddy covariance approach to CH_4 monitoring over two and
1027 a half decades. *Journal of Geophysical Research: Biogeosciences, 124*(3), 453–460.
1028 https://doi.org/10.1029/2018JG004796.
1029 Nadeau, D. F., Rousseau, A. N., Coursolle, C., Margolis, H. A., & Parlange, M. B. (2013).
1030 Summer methane fluxes from a boreal bog in northern Quebec, Canada, using eddy
1031 covariance measurements. *Atmospheric Environment, 81*, 464–474.
1032 https://doi.org/10.1016/j.atmosenv.2013.09.044.
1033 Nemitz, E., Mammarella, I., Ibrom, A., Aurela, M., Burba, G. G., Dengel, S., Gielen, B., Grelle,
1034 A., Heinesch, B., Herbst, M., & Others. (2018). Standardisation of eddy-covariance flux
1035 measurements of methane and nitrous oxide. *International Agrophysics, 32*(4), 517-549.
1036 https://doi:10.1515/intag-2017-0042.
1037 Nilsson, M. B., and Peichl, M. (2020). FLUXNET-CH4 SE-Deg Degero. Sweden.
1038 https://doi:10.18140/FLX/1669659.
1039 Oikawa, P. Y., Jenerette, G. D., Knox, S. H., Sturtevant, C., Verfaillie, J., Dronova, I.,
1040 Poindexter, C. M., Eichelmann, E., & Baldocchi, D. D. (2017). Evaluation of a hierarchy of
1041 models reveals importance of substrate limitation for predicting carbon dioxide and methane
1042 exchange in restored wetlands. *Journal of Geophysical Research: Biogeosciences, 122*(1),
1043 145–167. https://doi.org/10.1002/2016JG003438.
1044 Olefeldt, D., Turetsky, M. R., Crill, P. M., & David McGuire, A. (2013). Environmental and
1045 physical controls on northern terrestrial methane emissions across permafrost zones. *Global*
1046 *Change Biology, 19*(2), 589–603. https://doi.org/10.1111/gcb.12071.
1047 Olson, D. M., Dinerstein, E., Wikramanayake, E. D., Burgess, N. D., Powell, G. V. N.,
1048 Underwood, E. C., D'amico, J. A., Itoua, I., Strand, H. E., Morrison, J. C., Loucks, C. J.,

1049 Allnutt, T. F., Ricketts, T. H., Kura, Y., Lamoreux, J. F., Wettengel, W. W., Hedao, P., &
1050 Kassem, K. R. (2001). Terrestrial ecoregions of the world: A new map of life on Earth.
1051 *BioScience, 51*(11), 933. https://doi.org/10.1641/0006-3568(2001)051[0933:teotwa]2.0.co;2.
1052 Peltola, O., Vesala, T., Gao, Y., Räty, O., Alekseychik, P., Aurela, M., Chojnicki, B., Desai, A.
1053 R., Dolman, A. J., Euskirchen, E. S., Friborg, T., Göckede, M., Helbig, M., Humphreys, E.,
1054 Jackson, R. B., Jocher, G., Joos, F., Klatt, J., Knox, S. H., & Others. (2019). Monthly
1055 gridded data product of northern wetland methane emissions based on upscaling eddy
1056 covariance observations. *Earth System Science Data, 11*(3), 1263–1289.
1057 https://doi.org/10.5194/essd-11-1263-2019.
1058 Perryman, C. R., McCalley, C. K., Malhotra, A., Florencia Fahnestock, M., Kashi, N. N., Bryce,
1059 J. G., Giesler, R., & Varner, R. K. (2020). Thaw transitions and redox conditions drive
1060 methane oxidation in a permafrost peatland. *Journal of Geophysical Research:*
1061 *Biogeosciences, 125*(3). https://doi.org/10.1029/2019jg005526.
1062 Pugh, C. A., Reed, D. E., Desai, A. R., & Sulman, B. N. (2018). Wetland flux controls: how does
1063 interacting water table levels and temperature influence carbon dioxide and methane fluxes
1064 in northern Wisconsin? *Biogeochemistry, 137*(1), 15–25. https://doi.org/10.1007/s10533-
1065 017-0414-x.
1066 Pypker, T. G., Moore, P. A., Hribljan, J. A., & Chimner, R. (2013). Shifting environmental
1067 controls on CH4 fluxes in a sub-boreal peatland. *Biogeosciences, 10*, 7971-7981.
1068 https://doi.org/10.5194/bg-10-7971-2013.
1069 R Core Team. (2019). R: A language and environment for statistical computing. R Foundation
1070 for Statistical Computing. https://www.R-project.org/

1071 Rinne, J., Tuittila, E.-S., Peltola, O., Li, X., Raivonen, M., Alekseychik, P., Haapanala, S.,
1072 Pihlatie, M., Aurela, M., Mammarella, I., & Vesala, T. (2018). Temporal variation of
1073 ecosystem scale methane emission from a boreal fen in relation to temperature, water table
1074 position, and carbon dioxide fluxes. *Global Biogeochemical Cycles, 32*(7), 1087–1106.
1075 https://doi.org/10.1029/2017gb005747.
1076 Ruddell, B. L., Sturtevant, C., Kang, M., & Yu, R. (2008). ProcessNetwork Software (Version
1077 1.5) [Computer software]. Retrieved from
1078 https://github.com/ProcessNetwork/ProcessNetwork_Software.
1079 Ruddell, B. L., & Kumar, P. (2009). Ecohydrologic process networks: 1. Identification. *Water*
1080 *Resources Research, 45*(3). https://doi.org/10.1029/2008WR007279.
1081 Runge J., Bathiany, S., Bollt, E., Camps-Valls, G., Coumou, D., Deyle, E., Glymour, C.,
1082 Kretschmer, M., Mahecha, M., Muñoz-Marí, J., van Nes, E., Peters, J., Quax, R., Reichstein,
1083 M., Scheffer, M., Schölkopf, B., Spirtes, P., Sugihara, G., Sun, J., Zhang, K. & Zscheischler,
1084 J. (2019). Inferring causation from time series in Earth system sciences. *Nature:*
1085 *Communications, 10:2553*. https://doi.org/10.1038/s41467-019-10105-3.
1086 Runkle, B. R. K., Suvočarev, K., Reba, M. L., Reavis, C. W., Smith, S. F., Chiu, Y.-L., & Fong,
1087 B. (2019). Methane Emission Reductions from the Alternate Wetting and Drying of Rice
1088 Fields Detected Using the Eddy Covariance Method. Environmental Science & Technology,
1089 53(2), 671–681. https://doi.org/10.1021/acs.est.8b05535.
1090 Ryu, Youngryel, Kang, M., and Kim, J. (2020). FLUXNET-CH4 KR-CRK Cheorwon Rice
1091 paddy. Korea, Republic of. doi:10.18140/FLX/1669649.

1092 Sachs, T., Wille, C., Boike, J., & Kutzbach, L. (2008). Environmental controls on ecosystem-
1093 scale CH4 emission from polygonal tundra in the Lena River Delta, Siberia. *Journal of*
1094 *Geophysical Research: Biogeosciences, 113*(G3). https://doi.org/10.1029/2007JG000505.
1095 Sachs, T., Wille, C., Larmanou, E., and Franz, D. (2020). FLUXNET-CH4 DE-Zrk Zarnekow.
1096 Germany. https://doi:10.18140/FLX/1669636.
1097 Sakabe, A., Itoh, M., Hirano, T., and Kusin, K. (2020). FLUXNET-CH4 ID-Pag Palangkaraya
1098 undrained forest. Indonesia. https://doi:10.18140/FLX/1669643.
1099 Saunois, M., Stavert, A. R., Poulter, B., Bousquet, P., Canadell, J. G., Jackson, R. B., Raymond,
1100 P. A., Dlugokencky, E. J., Houweling, S., Patra, P. K., Ciais, P., Arora, V. K., Bastviken, D.,
1101 Bergamaschi, P., Blake, D. R., Brailsford, G., Bruhwiler, L., Carlson, K. M., Carrol, M.,
1102 Castaldi, S., Chandra, N., Crevoisier, C., Crill, P. M., Covey, K., Curry, C. L., Etiope, &
1103 Others. (2020). The global methane budget 2000--2017. *Earth System Science Data, 12*(3),
1104 1561–1623. https://doi.org/10.5194/essd-12-1561-2020.
1105 Savi, F., Di Bene, C., Canfora, L., Mondini, C., & Fares, S. (2016). Environmental and
1106 biological controls on CH_4 exchange over an evergreen Mediterranean forest. *Agricultural*
1107 *and Forest Meteorology, 226-227,* 67–79. https://doi.org/10.1016/j.agrformet.2016.05.014
1108 Schäfer, K. V. R., Tripathee, R., Artigas, F., Morin, T. H., & Bohrer, G. (2014). Carbon dioxide
1109 fluxes of an urban tidal marsh in the Hudson-Raritan estuary. *Journal of Geophysical*
1110 *Research: Biogeosciences, 119(*11), 2065–2081. https://doi.org/10.1002/2014jg002703.
1111 Schaller, C., Kittler, F., Foken, T., & Göckede, M. (2019). Characterisation of short-term
1112 extreme methane fluxes related to non-turbulent mixing above an Arctic permafrost
1113 ecosystem. *Atmospheric Chemistry and Physics, 19*(6), 4041–4059. https://doi:10.5194/acp-
1114 19-4041-2019.

1115 Schreiber, T. (2000). Measuring information transfer. *Physical Review Letters, 85*(2), 461–464.
1116 https://doi.org/10.1103/PhysRevLett.85.461.
1117 Seyfferth, A. L., Bothfeld, F., Vargas, R., Stuckey, J. W., Wang, J., Kearns, K., Michael, H. A.,
1118 Guimond, J., Yu, X., & Sparks, D. L. (2020). Spatial and temporal heterogeneity of
1119 geochemical controls on carbon cycling in a tidal salt marsh. *Geochimica et Cosmochimica*
1120 *Acta, 282*, 1–18. https://doi.org/10.1016/j.gca.2020.05.013.
1121 Sharma, A., & Mehrotra, R. (2014). An information theoretic alternative to model a natural
1122 system using observational information alone. *Water Resources Research, 50*(1), 650–660.
1123 https://doi.org/10.1002/2013wr013845.
1124 Song, C., Sun, L., Huang, Y., Wang, Y., & Wan, Z. (2011). Carbon exchange in a freshwater
1125 marsh in the Sanjiang Plain, northeastern China. *Agricultural and Forest Meteorology,*
1126 *151*(8), 1131–1138. https://doi.org/10.1016/j.agrformet.2011.04.001.
1127 Sonnentag, O., and Helbig, M. (2020). FLUXNET-CH4 CA-SCB Scotty Creek Bog. Canada.
1128 https://doi:10.18140/FLX/1669613.
1129 Sparks, J.P. (2020). FLUXNET-CH4 US-MAC MacArthur Agro-Ecology. United States.
1130 https://doi:10.18140/FLX/1669683.
1131 Strachan, I. B., Nugent, K. A., Crombie, S., & Bonneville, M.-C. (2015). Carbon dioxide and
1132 methane exchange at a cool-temperate freshwater marsh. *Environmental Research Letters,*
1133 *10*(6), 065006. https://doi.org/10.1088/1748-9326/10/6/065006.
1134 Strobl, C., Boulesteix, A.-L., Zeileis, A., & Hothorn, T. (2007). Bias in random forest variable
1135 importance measures: illustrations, sources, and a solution. *BMC Bioinformatics, 8*, 25.
1136 https://doi.org/10.1186/1471-2105-8-25.

1137 Strobl, C., Boulesteix, A.-L., Kneib, T., Augustin, T., & Zeileis, A. (2008). Conditional variable
1138 importance for random forests. *BMC Bioinformatics, 9:307.* doi:10.1186/1471-2105-9-307.
1139 Sturtevant, C., Ruddell, B. L., Knox, S. H., Verfaillie, J., Matthes, J. H., Oikawa, P. Y., &
1140 Baldocchi, D. (2016). Identifying scale-emergent, nonlinear, asynchronous processes of
1141 wetland methane exchange. *Journal of Geophysical Research: Biogeosciences, 121*(1), 188–
1142 204. https://doi.org/10.1002/2015JG003054.
1143 Wong, G.X., Melling, L., Tang, A.C.I., Aeries, E.B., Waili, J.W., Musin, K.K., Lo, K.S., and
1144 Kiew, F. (2020). FLUXNET-CH4 MY-MLM Maludam National Park. Malaysia.
1145 https://doi:10.18140/FLX/1669650.
1146 Tittel, J., Hüls, M., & Koschorreck, M. (2019). Terrestrial vegetation drives methane production
1147 in the sediments of two German reservoirs. *Scientific Reports, 9*(1), 15944.
1148 https://doi.org/10.1038/s41598-019-52288-1.
1149 Tokida, T. (2005). Ebullition of methane from peat with falling atmospheric pressure.
1150 *Geophysical Research Letters, 32*(13), 3257. https://doi.org/10.1029/2005GL022949.
1151 Tokida, T., Miyazaki, T., Mizoguchi, M., Nagata, O., Takakai, F., Kagemoto, A., & Hatano, R.
1152 (2007). Falling atmospheric pressure as a trigger for methane ebullition from peatland.
1153 *Global Biogeochemical Cycles, 21*(2). https://doi.org/10.1029/2006GB002790.
1154 Treat, C. C., Anthony Bloom, A., & Marushchak, M. E. (2018). Nongrowing season methane
1155 emissions-a significant component of annual emissions across northern ecosystems. *Global*
1156 *Change Biology, 24*(8), 3331–3343. https://doi.org/10.1111/gcb.14137.
1157 Trifunovic, B., Vázquez-Lule, A., Capooci, M., Seyfferth, A. L., Moffat, C., & Vargas, R.
1158 (2020). Carbon dioxide and methane emissions from temperate salt marsh tidal creek.

1159 *Journal of Geophysical Research: Biogeosciences, 125*(8), 84.
1160 https://doi.org/10.1029/2019JG005558.
1161 Tuovinen, J.-P., Aurela, M., Hatakka, J., Räsänen, A., Virtanen, T., Mikola, J., Ivakhov, V.,
1162 Kondratyev, V., & Laurila, T. (2019). Interpreting eddy covariance data from heterogeneous
1163 Siberian tundra: land cover-specific methane fluxes and spatial representativeness.
1164 *Biogeosciences, 16,* 255-274. https://doi.org/10.5194/bg-16-255-2019.
1165 Turetsky, M. R., Kotowska, A., Bubier, J., Dise, N. B., Crill, P., Hornibrook, E. R. C.,
1166 Minkkinen, K., Moore, T. R., Myers-Smith, I. H., Nykänen, H., Olefeldt, D., Rinne, J.,
1167 Saarnio, S., Shurpali, N., Tuittila, E.-S., Waddington, J. M., White, J. R., Wickland, K. P., &
1168 Wilmking, M. (2014). A synthesis of methane emissions from 71 northern, temperate, and
1169 subtropical wetlands. *Global Change Biology, 20*(7), 2183–2197.
1170 https://doi.org/10.1111/gcb.12580.
1171 Ueyama, M., Hirano, T., and Kominami, Y. (2020a). FLUXNET-CH4 JP-BBY Bibai bog. Japan.
1172 https://doi:10.18140/FLX/1669646.
1173 Ueyama, M., Yazaki, T., Hirano, T., Futakuchi, Y., & Okamura, M. (2020b). Environmental
1174 controls on methane fluxes in a cool temperate bog. *Agricultural and Forest Meteorology,*
1175 *281,* 107852. https://doi.org/10.1016/j.agrformet.2019.107852.
1176 Updegraff, K., Bridgham, S. D., Pastor, J., Weishampel, P., & Harth, C. (2001). Response of
1177 CO_2 and CH_4 emissions from peatlands to warming and water table manipulation.
1178 *Ecological Applications, 11*(2), 311. https://doi.org/10.2307/3060891.
1179 Valach, A., Szutu, D., Eichelmann, E., Knox, S., Verfaillie, J., and Baldocchi, D. (2020).
1180 FLUXNET-CH4 US-Tw1 Twitchell Wetland West Pond. United States.
1181 https://doi:10.18140/FLX/1669696.

1182 Van der Nat, F.-J., & Middelburg, J. J. (2000). Methane emission from tidal freshwater marshes.
1183 *Biogeochemistry, 49*(2), 103–121. https://doi.org/10.1023/A:1006333225100.
1184 Vesala, T., Tuittila, E.-S., Mammarella, I., and Alekseychik, P. (2020a). FLUXNET-CH4 FI-Si2
1185 Siikaneva-2 Bog. Finland. https://doi:10.18140/FLX/1669639.
1186 Vesala, T., Tuittila, E.-S., Mammarella, I., and Rinne, J. (2020b). FLUXNET-CH4 FI-Sii
1187 Siikaneva. Finland. https://doi:10.18140/FLX/1669640.
1188 Villa, J. A., Ju, Y., Stephen, T., Rey-Sanchez, C., Wrighton, K. C., & Bohrer, G. (2020).
1189 Plant-mediated methane transport in emergent and floating-leaved species of a temperate
1190 freshwater mineral-soil wetland. *Limnology and Oceanography, 65*(7), 1635–1650.
1191 https://doi.org/10.1002/lno.11467.
1192 Villa, J. A., Y. Ju, T. Yazbeck, S. Waldo, K. C. Wrighton, and G. Bohrer. (2021). Ebullition
1193 dominates methane fluxes from the water surface across different ecohydrological patches in
1194 a temperate freshwater marsh at the end of the growing season. *Science of the Total*
1195 *Environment*, *767*, 144498. doi:https://doi.org/10.1016/j.scitotenv.2020.144498.
1196 Vourlitis, G., Dalmagro, H., Nogueira, J.S., Johnson M., and Arruda, P. (2020). FLUXNET-CH4
1197 BR-Npw Northern Pantanal Wetland. Brazil. https://doi:10.18140/FLX/1669368.
1198 Wen, X., Unger, V., Jurasinski, G., Koebsch, F., Horn, F., Rehder, G., Sachs, T., Zak, D.,
1199 Lischeid, G., Knorr, K.-H., Böttcher, M. E., Winkel, M., Bodelier, P. L. E., & Liebner, S.
1200 (2018). Predominance of methanogens over methanotrophs in rewetted fens characterized by
1201 high methane emissions. *Biogeosciences, 15(*21), 6519–6536. https://doi.org/10.5194/bg-15-
1202 6519-2018.
1203 Wood, S. N. (2011). Fast stable restricted maximum likelihood and marginal likelihood
1204 estimation of semiparametric generalized linear models. *Journal of the Royal Statistical*

*Society: Series B (Statistical Methodology), 73(*1), 3–36. https://doi.org/10.1111/j.1467-9868.2010.00749.x.

Wright, M. N., & Ziegler, A. (2017). ranger: A fast implementation of random forests for high dimensional data in C++ and R. *Journal of Statistical Software, 77*(1), pp. 1–17. https://doi.org/10.18637/jss.v077.i01.

Yang, W. H., McNicol, G., Teh, Y. A., Estera-Molina, K., Wood, T. E., & Silver, W. L. (2017). Evaluating the classical versus an emerging conceptual model of peatland methane dynamics. *Global Biogeochemical Cycles, 31*(9), 1435-1453. https://doi.org/10.1002/2017GB005622.

Yvon-Durocher, G., Allen, A. P., Bastviken, D., Conrad, R., Gudasz, C., St-Pierre, A., Thanh-Duc, N., & del Giorgio, P. A. (2014). Methane fluxes show consistent temperature dependence across microbial to ecosystem scales. *Nature, 507*(7493), 488–491. https://doi.org/10.1038/nature13164.

Zhao, J., Zhou, Y., Zhang, X., & Chen, L. (2016). Part mutual information for quantifying direct associations in networks. *Proceedings of the National Academy of Sciences, 113*(18), 5130–5135. https://doi.org/10.1073/pnas.1522586113.

Zona, D., Gioli, B., Commane, R., Lindaas, J., Wofsy, S. C., Miller, C. E., Dinardo, S. J., Dengel, S., Sweeney, C., Karion, A., -W. Chang, R. Y., Henderson, J. M., Murphy, P. C., Goodrich, J. P., Moreaux, V., Liljedahl, A., Watts, J. D., Kimball, J. S., Lipson, D. A., & Oechel, W. C. (2016). Cold season emissions dominate the Arctic tundra methane budget. *Proceedings of the National Academy of Sciences, 113(*1), 40–45. https://doi.org/10.1073/pnas.1516017113.

Tables

Table 1. Physical and biological predictors included in this analysis and references from studies that have previously identified these variables as predictors of methane fluxes (FCH4). Here we consider variables that have a direct influence on methane (CH_4) production, consumption and/or transport (white cells associated with each predictor), and variables that represent a proxy or are correlated with a process that has a direct influence on FCH4 (gray cells). We also include scales at which we hypothesize that these predictors will be dominant.

Predictor	Mechanism(s) & hypothesized scale	References
Biological predictors		
Gross primary productivity (GPP)	• Oxygenation of zone around roots (direct driver of CH_4 consumption) (*diel to seasonal scale*) • Carbon substrate for methanogens (i.e., root exudates, root mortality, plant residue) (proxy for CH_4 production) (*diel to seasonal scale*) • Coupling between FCH4 and leaf photosynthesis may indicate that FCH4 is regulated by stomatal conductance (proxy for CH_4 transport) (*diel scale*) • CH_4 transport through aerenchymatous vegetation will lead to coupling between vegetation development (e.g., stalk diameter, Leaf area index (LAI)) and FCH4 since seasonal development of the vegetation will increase the available aerenchyma area (proxy for CH_4 transport) (*seasonal scale*)	(Hatala et al., 2012b; Malhotra & Roulet, 2015; Knox et al., 2016; Rinne et al., 2018)
Ecosystem respiration (RECO)	• May describe similar effects to those that influence CH_4 production/consumption/flux (proxy for FCH4) (*diel to seasonal scale*) • Breakdown of complex carbon compounds provides simple carbon substrates that fuel methanogenesis and CH_4 production (*diel to seasonal scale*)	(Villa et al., 2020)
Net ecosystem exchange (NEE)	• NEE is linked to plant activity (GPP) (direct effect and proxy for FCH4) and respiration (RECO) (proxy for FCH4) (*diel to seasonal scale*)	(Pypker et al., 2013)
Biological and physical predictors		
Latent heat turbulent flux (LE)	• Evaporation of water and CH_4 volatilization from the water and plant surfaces are driven by similar physical mechanisms and tend to covary (proxy for CH_4 transport) (*diel to seasonal scale*) • LE is linked to plant activity (e.g., LAI is a strong determinant of LE) (proxy for CH_4 transport) (*seasonal scale*) • Influence of vapor pressure deficit (VPD)/humidity gradients on pressurized ventilation in aerenchymatous vegetation (proxy for CH_4 transport) (*diel scale*) • In some species, stomatal conductance of water vapor from the vegetation is correlated with CH_4 transport through plant tissue (proxy for CH_4 transport) (*diel scale*)	(Morin et al., 2014; Savi et al., 2016; Sturtevant et al., 2016; Morin, 2019; Villa et al., 2020)

Physical predictors		
Air temperature (TA)	• Temperature-dependence of microbial CH_4 production and consumption (direct driver of CH_4 production and consumption) (*multiday to seasonal scale*) • Influence on diffusive transport in plants (direct driver of CH_4 transport) (*multiday to seasonal scale*)	(Pugh et al., 2018, Koebsch et al. 2015)
Soil temperature (TS)	• Temperature-dependence of microbial processes controlling CH_4 production and oxidation (direct driver of CH_4 production and consumption) (*multiday to seasonal scale*) • Influence on soil diffusion and ebullition of CH_4 (direct driver of CH_4 transport) (*multiday to seasonal scale*)	(Olefeldt et al., 2013; Turetsky et al., 2014; Goodrich et al., 2015; Zona et al., 2016)
Water table depth (WTD)	• Influence on soil redox conditions (direct driver of CH_4 production and consumption) (*multiday to seasonal scale*) • Influence on slow vs. rapid diffusion of CH_4 through water vs. soils, respectively (CH_4 transport) (*diel to multiday scale*) • Influence on the rates of ebullition (CH_4 transport) (*diel to multiday scale*)	(Olefeldt et al., 2013; Turetsky et al., 2014; Goodrich et al., 2015; Bansal et al. 2020;Villa et al 2021)
Incoming shortwave radiation (SW_IN)	• Influence on TA, TS, GPP, LE, and mixing of the water column (proxy for FCH4) (*diel to seasonal scale*) • Influence of light on plant activity (proxy for CH_4 transport) (*diel and seasonal scale*)	(Savi et al., 2016)
Vapor pressure deficit (VPD)	• Influence on pressurized ventilation of CH_4 in aerenchymatous vegetation (direct influence on CH_4 transport) (*diel scale*) • Influence on GPP and LE (proxy for FCH4) (*diel to seasonal scale*) • Covaries with near-surface CH_4 concentration in the air through boundary layer growth and depth (proxy for CH_4 transport) (*diel scale*)	(Chanton et al., 1997; Sturtevant et al., 2016; Chen et al., 2019; Morin, 2019)
Friction velocity (USTAR)	• Near surface turbulence can influence ebullition and diffusion, and increased turbulence can lead to increased aeration and transient flushing of CH_4 stored in soil (direct driver of CH_4 transport) (*diel to multiday scale*)	(Sachs et al., 2008; Nadeau et al., 2013, Koebsch et al. 2015)
Atmospheric pressure (PA)	• Atmospheric pressure (falling pressure) as a trigger for methane ebullition (direct driver of CH_4 transport) (*diel to multiday scale*)	(Tokida, 2005; Tokida et al., 2007; Sachs et al., 2008; Linkhorst et al., 2020;)
Wind direction (WD)*	• Related to site heterogeneity (indirect relationship with FCH4) (*diel to seasonal scale*) *Note that WD was separated into sine and cosine of wind direction (sinWD, cosWD) to represent WD as a continuous function.	(Jammet et al., 2017; Tuovinen et al., 2019)

Table 2. Description of study sites. For vegetation cover, 0 = absent and 1 = present.

Site ID	Country	Lat	Long	Wetland Type	Biome	Management regime	Start year	End year	Mean CH_4 flux (nmol m^{-2} s^{-1})	Median CH_4 flux (nmol m^{-2} s^{-1})
CA-SCB	Canada	61.308	-121.298	Bog	Boreal	Natural	2014	2016	53.71	52.02
FI-Si2	Finland	61.837	24.197	Bog	Boreal	Natural	2012	2016	46.11	34.40
US-Uaf	USA	64.866	-147.856	Bog	Boreal	Natural	2011	2018	2.66	1.80
JP-BBY	Japan	43.323	141.811	Bog	Temperate	Natural	2015	2018	64.99	58.13
NZ-Kop	New Zealand	-37.388	175.554	Bog	Temperate	Natural	2012	2015	47.03	43.84
FI-Sii	Finland	61.833	24.193	Fen	Boreal	Natural	2013	2018	35.40	19.10
SE-Deg	Sweden	64.182	19.557	Fen	Boreal	Natural	2014	2018	31.65	21.63
US-Los	USA	46.083	-89.979	Fen	Boreal	Natural	2014	2018	18.43	8.63
DE-Hte	Germany	54.210	12.176	Fen	Temperate	Restored	2011	2018	166.88	123.77
DE-Zrk	Germany	53.876	12.889	Fen	Temperate	Restored	2016	2018	80.70	21.30
FI-Lom	Finland	67.997	24.209	Fen	Temperate	Natural	2006	2010	49.71	31.50
US-Myb	USA	38.050	-121.765	Marsh	Temperate	Restored	2011	2018	154.70	130.42
US-OWC	USA	41.380	-82.513	Marsh	Temperate	Natural	2015	2016	627.33	540.92
US-Tw1	USA	38.107	-121.647	Marsh	Temperate	Restored	2012	2018	170.80	149.84
US-Tw4	USA	38.103	-121.641	Marsh	Temperate	Restored	2014	2018	98.63	79.88
US-WPT	USA	41.465	-82.996	Marsh	Temperate	Natural	2011	2013	127.61	35.90
JP-Mse	Japan	36.054	140.027	Rice	Temperate	Managed	2012	2012	59.35	35.00
KR-CRK	Korea	38.201	127.251	Rice	Temperate	Managed	2015	2018	98.80	37.10
US-Twt	USA	38.109	-121.653	Rice	Temperate	Managed	2009	2017	37.71	14.29
US-MAC	USA	27.163	-81.187	Drained	Temperate	Managed	2013	2016	52.8	20.2
BR-Npw	Brazil	-16.498	-56.412	Swamp	Tropical & Subtropical	Natural	2015	2016	63.55	15.42
ID-Pag	Indonesia	-2.32	113.9	Swamp	Tropical & Subtropical	Natural	2016	2017	-0.42	0.49
MY-MLM	Malaysia	1.454	111.150	Swamp	Tropical & Subtropical	Natural	2014	2015	28.94	17.76

1241 Table 2. (cont.)

Site ID	Moss (None)	Moss (Brown)	Moss (*Sphagnum*)	Aerenchy-matous	Erica-ceous Shrub	Tree	Data DOI/location	Data DOI Reference
CA-SCB	0	0	1	1	1	0	10.18140/FLX/1669613	Sonnentag et al., 2020
FI-Si2	0	0	1	1	1	1	10.18140/FLX/1669639	Vesala et al., 2020b
US-Uaf	0	1	1	1	1	1	10.18140/FLX/1669701	Iwata et al., 2020b
JP-BBY	0	0	1	1	1	0	10.18140/FLX/1669646	Ueyama et al., 2020a
NZ-Kop	0	0	1	1	0	0	10.18140/FLX/1669652	Campbell et al., 2020
FI-Sii	0	0	1	1	0	0	10.18140/FLX/1669640	Vesala et al., 2020a
SE-Deg	0	0	1	1	1	0	10.18140/FLX/1669659	Nilsson et al., 2020
US-Los	1	0	0	1	1	1	10.18140/FLX/1669682	Desai et al., 2020
DE-Hte	1	0	0	1	0	0	10.18140/FLX/1669634	Koebsch et al., 2020b
DE-Zrk	1	0	0	1	0	0	10.18140/FLX/1669636	Sachs et al., 2020
FI-Lom	0	1	1	1	1	0	10.18140/FLX/1669638	Aurela et al., 2020
US-Myb	1	0	0	1	0	0	10.18140/FLX/1669685	Matthes et al., 2020
US-OWC	1	0	0	1	0	0	10.18140/FLX/1669690	Bohrer et al., 2020
US-Tw1	1	0	0	1	0	0	10.18140/FLX/1669696	Valach et al., 2020
US-Tw4	1	0	0	1	0	0	10.18140/FLX/1669698	Eichelmann et al., 2020
US-WPT	1	0	0	1	0	0	10.18140/FLX/1669702	Chen et al., 2020
JP-Mse	1	0	0	1	0	0	10.18140/FLX/1669647	Iwata, 2020a
KR-CRK	1	0	0	1	0	0	10.18140/FLX/1669649	Ryu et al., 2020
US-Twt	1	0	0	1	0	0	10.18140/FLX/1669700	Knox et al., 2020
US-MAC	1	0	0	1	0	0	10.18140/FLX/1669683	Sparks 2020
BR-Npw	1	0	0	1	0	1	10.18140/FLX/1669368	Vourlitis et al., 2020
ID-Pag	1	0	0	1	0	1	10.18140/FLX/1669643	Sakabe et al., 2020
MY-MLM	1	0	0	0	0	1	10.18140/FLX/1669650	Wong et al., 2020

Table 3. Summary of top three dominant significant predictors ($p < 0.05$) of methane flux across sites for each time scale and statistical methods of correlation, synchronous and maximum information theory (IR), generalized additive modeling (GAM) and random forest (RF). Variables are defined in Table 1. Note that significance was not assessed for RF based on the method of estimating variable importance. Analyses for 'Seasonal', 'Multiday' and 'Diel' time scales were on wavelet transformed data.

	Seasonal			Multiday			Diel			Daily average		
Statistical Method	**#1**	**#2**	**#3**	**#1**	**#2**	**#3**	**#1**	**#2**	**#3**	**#1**	**#2**	**#3**
Correlation	TS	LE	TA	PA	TA	LE	LE	NEE	SW_IN	TS	TA	GPP
Synchronous IR	TS	TA	LE	TS	TA	PA	LE	NEE	GPP	TS	TA	GPP
Maximum IR	TS	TA	LE	TS	TA	LE	NEE	LE	GPP	TS	GPP	NEE
GAM	TS	TA	LE	TA	sinWD	TS	LE	NEE	SW_IN	TA	TS	GPP
RF	TS	NEE	TA	WTD	TS	TA	NEE	LE	GPP	TS	GPP	WTD

Figure legends

Figure 1. Locations of non-tidal, freshwater wetland eddy covariance sites included in this analysis of methane flux, with sites colored by wetland type. More information on these sites is provided in Table 2.

Figure 2. Variance of methane flux (FCH4) wavelet coefficients at each time scale of interest as a percentage of the total variance for all sites in Table 2. The color of site labels indicates wetland type as defined in Table 2, and include bogs (pink), drained (orange), fens (green), marshes (blue), rice paddies (red), and swamps (gray). Note that the time scales of variation are described in Section 2.2.1. See Table 2 for site information and Table 1 for predictor variable information.

Figure 3. Heatmap of normalized, maximum relative mutual information (IR) between methane flux (FCH4) and biophysical variables within sites for the (a) seasonal scale, (b) multiday scale, (c) diel scale, and (d) daily average scale. Analyses for a-c were conducted on wavelet transformed data. Colors range from light yellow (lowest normalized IR) to dark red (highest normalized IR). Note that non-significant IR values are shaded white. Sites are colored by wetland type as defined in Table 2 and Fig. 1, which includes bogs (pink), drained (orange), fens (green), marshes (blue), rice paddies (red), and swamps (gray). See Table 2 for site information and Table 1 for predictor variable information.

Figure 4. Biplots showing the two largest components from the principal component analysis of the matrix of normalized, maximum IR at the (a) seasonal scale, and (b) multiday scale. In (a) sites are colored by wetland type and the size of the dots represent the ratio of the standard deviation (SD) in WTD to SD in TA at the site. Direction and importance of normalized, maximum IR is illustrated by the vectors. See Table 2 for site information and Table 1 for predictor variable information.

Figure 5. Histogram of the lag (inferred from maximum IR) between methane flux (FCH4) and (a) WTD (7 sites, median lag = 17 days and mean lag = 18.3 days), (b) TA (19 sites, median lag = 8 days and mean lag = 10.8 days), (c) TS at depth where IR at zero lag was greatest (17 sites, median lag = 5 days and mean lag = 5.4 days), (d) LE (16 sites, median lag = 17 days and mean lag = 20.2 days), and (e) GPP (10 sites, median lag = 12.5 days and mean lag = 20.7 days). Red line indicates zero lag, dashed black line represents median lag across sites, and solid black line represents mean lag across sites. Note that the variable number of sites is due to the fact that we only included sites where the driver of interest (i.e., WTD, TA or TS) was statistically significant and in the top five highest ranked predictors. See Table 2 for site information and Table 1 for predictor variable information.

Figure 6. Relative mutual information (IR) as a function of lag between wavelet transformed multiday methane flux (FCH4) and (a) PA, (c) temperature (TA or TS depending on which had the highest IR, and (e) WTD. For ease of visualization only sites where drivers were the top predictor of multiday FCH4 are included here. Vertical lines represent zero lag ($\tau = 0$) (dotted red line), and the mean (black line) and median (dashed black line) lag of maximum IR across sites. IR across all sites and lags were significant. Wavelet detail reconstruction of FCH4 and (b) PA (note the negative sign for ease of visualization) for JP-BBY, (d) TS for DE-Zrk, and (f)

1295 WTD for US-Tw1. Note that the mean is removed in wavelet detail reconstructions, therefore the
1296 y-axes are relative rather than absolute. Panels (b), (d), and (f) illustrate an example of the
1297 relationships observed in panels (a), (c), and (e). See Table 2 for site information and Table 1 for
1298 predictor information.

1299 Figure 7. Average diel variation in the wavelet detail reconstruction for methane flux (FCH4)
1300 and the predictor at maximum IR, with the lead or lag (τ) at which it occurred (in hours, positive
1301 and negative values indicate FCH4 lagging and leading predictors, respectively). Note that the
1302 mean is removed in wavelet detail reconstructions; therefore, the y-axes are relative rather than
1303 absolute. Sites are colored by wetland type as defined in Table 2, bogs (pink), drained (orange),
1304 fens (green), marshes (blue), rice paddies (red), and swamps (gray). Also note that we used net
1305 ecosystem production (NEP) (i.e., -net ecosystem exchange [NEE]) for ease of visualization.
1306 See Table 2 for site information and Table 1 for predictor variable information.
1307
1308 Figure 8. Conceptual diagram summarizing the dominant predictors of methane flux (FCH4)
1309 across methods, including median leads and lags identified from the IR analysis, across sites and
1310 time scales. Variables are sorted by importance by the most dominant (outer ring) to least (inner
1311 ring). Directional arrows indicate significant leads (right arrow) and lags (left arrow) of
1312 corresponding predictor with the same color. Predictors are air temperature (TA), soil
1313 temperature (TS), water table depth (WTD), latent heat turbulent flux (LE), gross primary
1314 productivity (GPP), net ecosystem exchange (NEE), air pressure (PA), and vapor pressure deficit
1315 (VPD); more predictor details in Table 1.

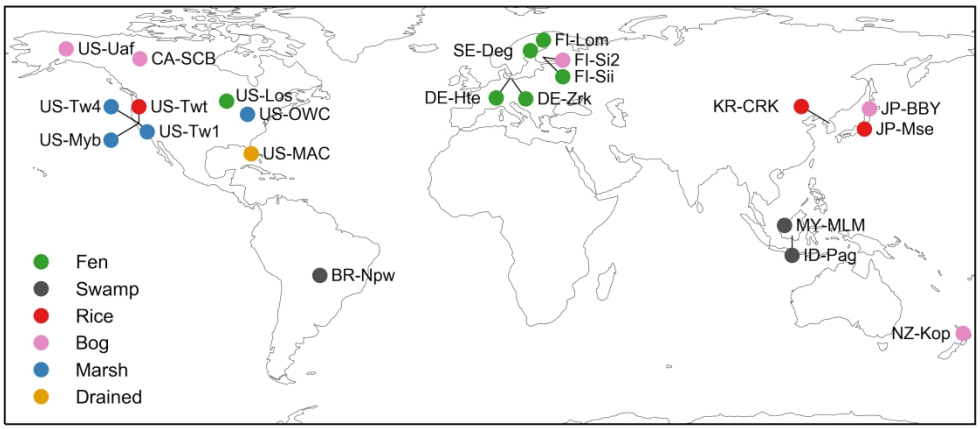

Figure 1. Locations of non-tidal, freshwater wetland eddy covariance sites included in this analysis of methane flux, with sites colored by wetland type. More information on these sites is provided in Table 2.

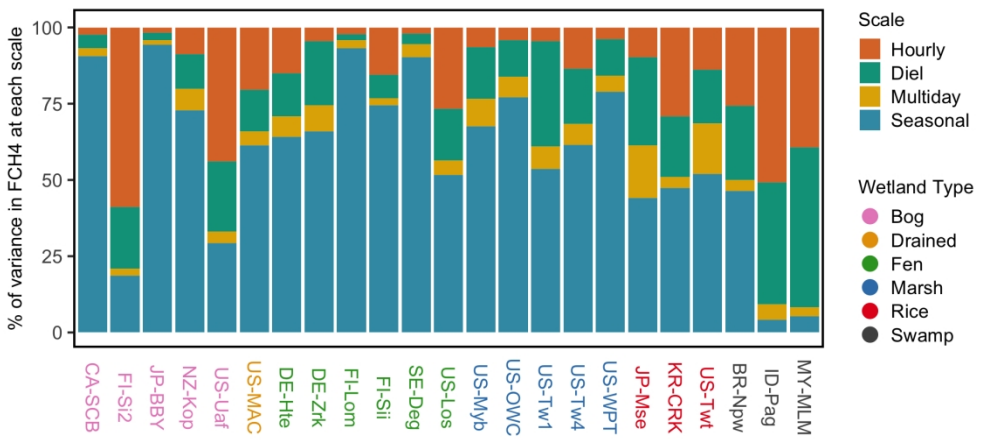

Figure 2. Variance of methane flux (FCH4) wavelet coefficients at each time scale of interest as a percentage of the total variance for all sites in Table 2. The color of site labels indicates wetland type as defined in Table 2, and include bogs (pink), drained (orange), fens (green), marshes (blue), rice paddies (red), and swamps (gray). Note that the time scales of variation are described in Section 2.2.1. See Table 2 for site information and Table 1 for predictor variable information.

704x333mm (72 x 72 DPI)

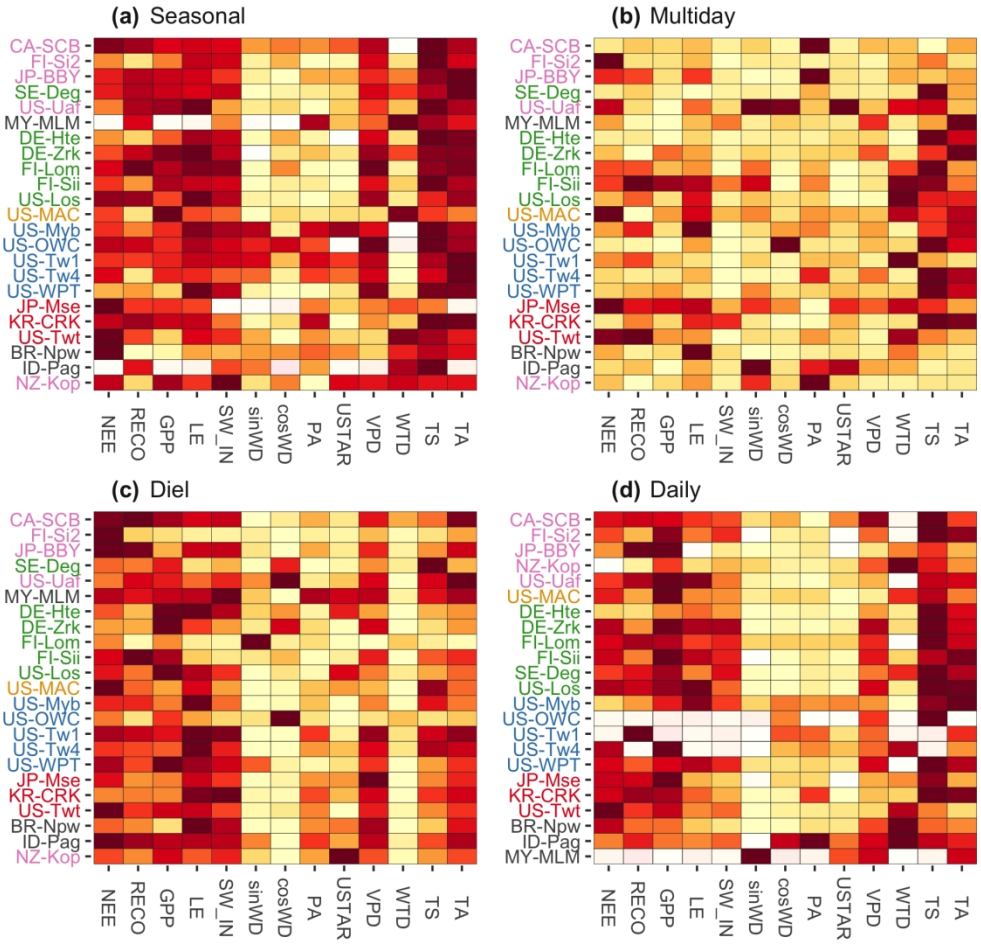

Figure 3. Heatmap of normalized, maximum relative mutual information (IR) between methane flux (FCH4) and biophysical variables within sites for the (a) seasonal scale, (b) multiday scale, (c) diel scale, and (d) daily average scale. Analyses for a-c were conducted on wavelet transformed data. Colors range from light yellow (lowest normalized IR) to dark red (highest normalized IR). Note that non-significant IR values are shaded white. Sites are colored by wetland type as defined in Table 2 and Fig. 1, which includes bogs (pink), drained (orange), fens (green), marshes (blue), rice paddies (red), and swamps (gray). See Table 2 for site information and Table 1 for predictor variable information.

704x666mm (72 x 72 DPI)

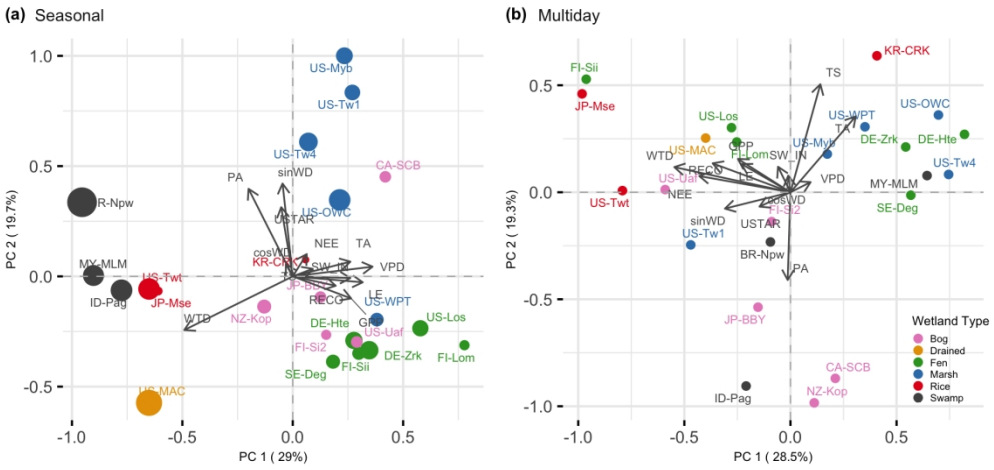

Figure 4. Biplots showing the two largest components from the principal component analysis of the matrix of normalized, maximum IR at the (a) seasonal scale, and (b) multiday scale. In (a) sites are colored by wetland type and the size of the dots represent the ratio of the standard deviation (SD) in WTD to SD in TA at the site. Direction and importance of normalized, maximum IR is illustrated by the vectors. See Table 2 for site information and Table 1 for predictor variable information.

704x333mm (72 x 72 DPI)

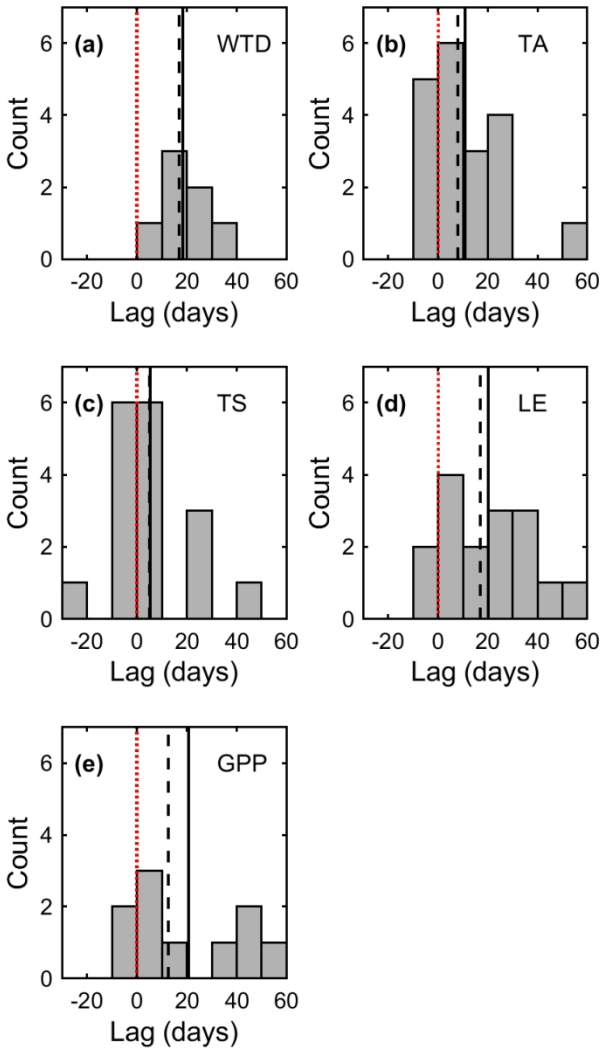

Figure 5. Histogram of the lag (inferred from maximum IR) between methane flux (FCH4) and (a) WTD (7 sites, median lag = 17 days and mean lag = 18.3 days), (b) TA (19 sites, median lag = 8 days and mean lag = 10.8 days), (c) TS at depth where IR at zero lag was greatest (17 sites, median lag = 5 days and mean lag = 5.4 days), (d) LE (16 sites, median lag = 17 days and mean lag = 20.2 days), and (e) GPP (10 sites, median lag = 12.5 days and mean lag = 20.7 days). Red line indicates zero lag, dashed black line represents median lag across sites, and solid black line represents mean lag across sites. Note that the variable number of sites is due to the fact that we only included sites where the driver of interest (i.e., WTD, TA or TS) was statistically significant and in the top five highest ranked predictors. See Table 2 for site information and Table 1 for predictor variable information.

80x140mm (300 x 300 DPI)

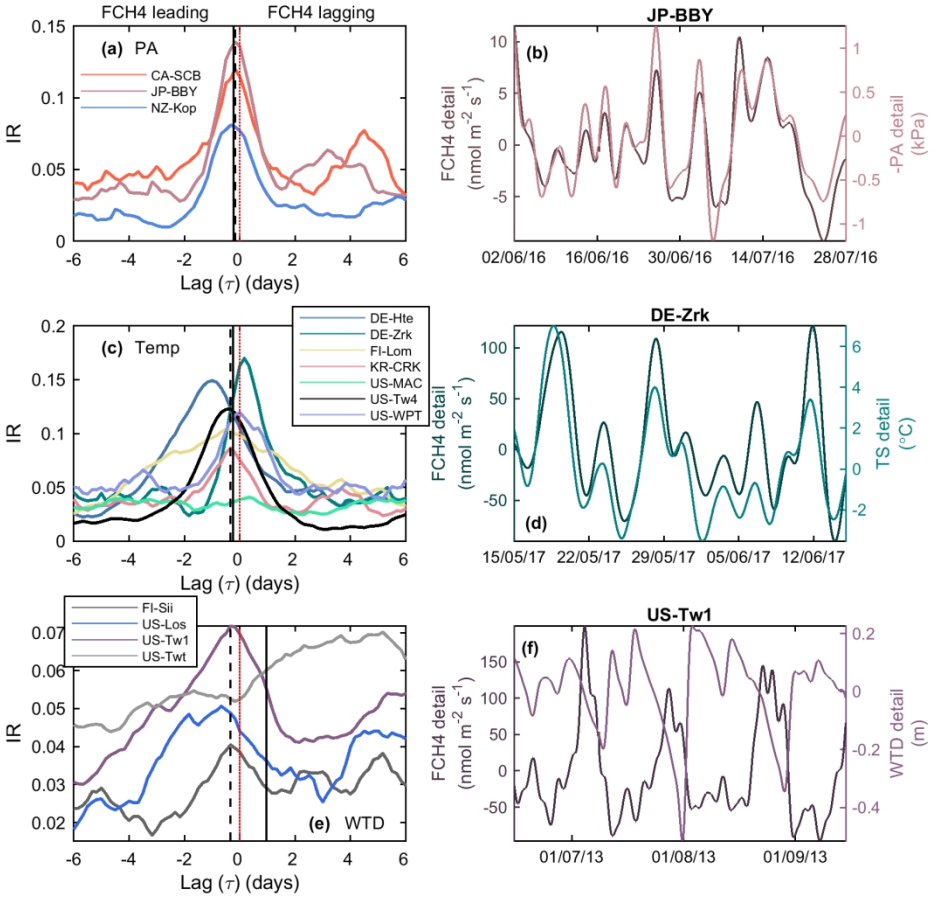

Figure 6. Relative mutual information (IR) as a function of lag between wavelet transformed multiday methane flux (FCH4) and (a) PA, (c) temperature (TA or TS depending on which had the highest IR, and (e) WTD. For ease of visualization only sites where drivers were the top predictor of multiday FCH4 are included here. Vertical lines represent zero lag (�� = 0) (dotted red line), and the mean (black line) and median (dashed black line) lag of maximum IR across sites. IR across all sites and lags were significant. Wavelet detail reconstruction of FCH4 and (b) PA (note the negative sign for ease of visualization) for JP-BBY, (d) TS for DE-Zrk, and (f) WTD for US-Tw1. Note that the mean is removed in wavelet detail reconstructions, therefore the y-axes are relative rather than absolute. Panels (b), (d), and (f) illustrate an example of the relationships observed in panels (a), (c), and (e). See Table 2 for site information and Table 1 for predictor information.

160x160mm (300 x 300 DPI)

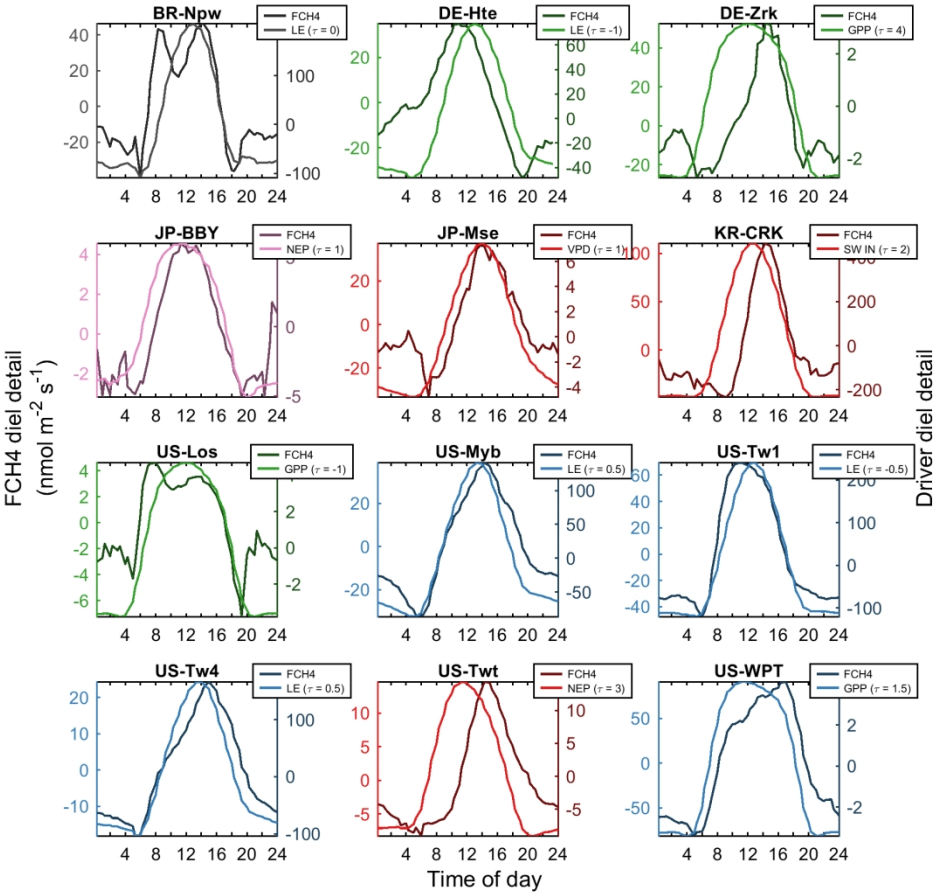

Figure 7. Average diel variation in the wavelet detail reconstruction for methane flux (FCH4) and the predictor at maximum IR, with the lead or lag (��) at which it occurred (in hours, positive and negative values indicate FCH4 lagging and leading predictors, respectively). Note that the mean is removed in wavelet detail reconstructions; therefore, the y-axes are relative rather than absolute. Sites are colored by wetland type as defined in Table 2, bogs (pink), drained (orange), fens (green), marshes (blue), rice paddies (red), and swamps (gray). Also note that we used net ecosystem production (NEP) (i.e., -net ecosystem exchange [NEE]) for ease of visualization. See Table 2 for site information and Table 1 for predictor variable information.

160x160mm (300 x 300 DPI)

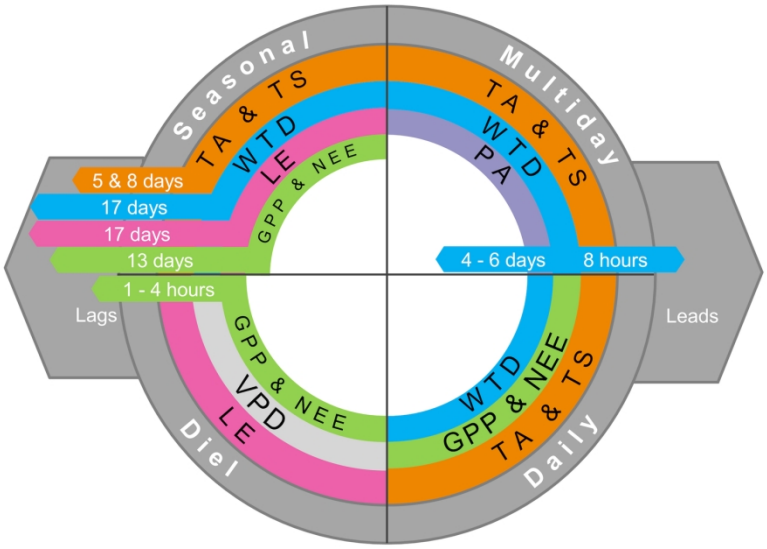

Figure 8. Conceptual diagram summarizing the dominant predictors of methane flux (FCH4) across methods, including median leads and lags identified from the IR analysis, across sites and time scales. Variables are sorted by importance by the most dominant (outer ring) to least (inner ring). Directional arrows indicate significant leads (right arrow) and lags (left arrow) of corresponding predictor with the same color. Predictors are air temperature (TA), soil temperature (TS), water table depth (WTD), latent heat turbulent flux (LE), gross primary productivity (GPP), net ecosystem exchange (NEE), air pressure (PA), and vapor pressure deficit (VPD); more predictor details in Table 1.

168x94mm (300 x 300 DPI)